Final Technical Report

April 23, 1996

Reporting Period: 01 July 1992 - 30 April 1995

Optoelectronic Technology Consortium

Sponsored by:

Defense Advanced Research Projects Agency
Microelectronics Technology Office

[PRECOMPETITIVE CONSORTIUM FOR OPTOELECTRONIC INTERCONNECT TECHNOLOGY]

ARPA Order No. 8351C

Issued by DARPA/CMO under Contract #MDA972-92-C-0071

Prepared by:

Dr. Mary Hibbs-Brenner (PI)
Honeywell Systems and Research Center
(612) 887-6466
fax: (612) 887-4517
MHIBBSBREN @ P01.MN09.HONEYWELL.COM

REPORT DOCUMENTATION PAGE

Form Approved
OMB No. 0704-0188

1. AGENCY USE ONLY (Leave blank)	2. REPORT DATE	3. REPORT TYPE AND DATES COVERED
	April 23, 1996	Final Technical Report 01 July 1992-30 April 1995

4. TITLE AND SUBTITLE

Optoelectronic Technology Consortium

5. FUNDING NUMBERS

ARPA order no. 8351C
Contract #: MDA972-92-C-0071

6. AUTHOR(S)

Mary Hibbs-Brenner

7. PERFORMING ORGANIZATION NAME(S) AND ADDRESS(ES)

Honeywell Technology Center
3660 Technology Drive
Minneapolis, MN 55418

8. PERFORMING ORGANIZATION REPORT NUMBER

9. SPONSORING/MONITORING AGENCY NAME(S) AND ADDRESS(ES)

Defense Advanced Research Projects Agency
3791 North Fairfax Drive
Arlington, VA 22203-1714

10. SPONSORING/MONITORING AGENCY REPORT NUMBER

11. SUPPLEMENTARY NOTES

12a. DISTRIBUTION/AVAILABILITY STATEMENT

Unlimited distribution

12b. DISTRIBUTION CODE

13. ABSTRACT *(Maximum 200 words)*

This report describes the results of Honeywell's effort under the Optoelectronic Technology Consortium project. The program involved a consortium of Honeywell, AT&T, IBM and Martin Marietta. The overall goal of the program was to develop parallel fiber optic data link component and packaging technology and to demonstrate a link possessing 32 channels, each operating a 500 Mbps for an aggregate data rate of 16 Gbps. Baseline and alternate technologies were investigated. Honeywell's effort included: 1) the development of AlGaAs waveguide based four element electro-optic modulator arrays as an alternate transmitter technology, 2) packaging technology required to couple single mode fiber to, and multi-mode fiber from, the modulator array, and 3) a polymer waveguide based board level interconnect demonstration included an expanded beam connector feasibility study. Partway through the program we added a task to develop a second source capability for the Vertical Cavity Surface Emitting Lasr (VCSEL) arrays. During the program we demonstrated multi-gigaherz bandwidth modulator arrays with a contrast ratio >10dB, and a voltage-length product of approximately 5.5V-cm. The packaging technique developed allowed one to maintain a 1 dB additional coupling loss over the 0 to +125 deg C temperature range. The polymer waveguide demonstration showed that 60 optical waveguide channels could be coupled from board to board through a 3mm connector with a fraction of a millimeter board to board alignment tolerance. We also demonstrated the fabrication of VCSEL arrays using MOCVD as the epitaxial layer growth technology.

14. SUBJECT TERMS	15. NUMBER OF PAGES
optoelectronic components, optoelectronic packaging electro-optic modulators, polymer waveguides, vertical cavity surface emitting lasers	16. PRICE CODE

17. SECURITY CLASSIFICATION OF REPORT	18. SECURITY CLASSIFICATION OF THIS PAGE	19. SECURITY CLASSIFICATION OF ABSTRACT	20. LIMITATION OF ABSTRACT
unclassified	unclassified	unclassified	unlimited distribution

39464

GENERAL INSTRUCTIONS FOR COMPLETING SF 298

The Report Documentation Page (RDP) is used in announcing and cataloging reports. It is important that this information be consistent with the rest of the report, particularly the cover and title page. Instructions for filling in each block of the form follow. It is important to ***stay within the lines*** to meet ***optical scanning requirements***.

Block 1. Agency Use Only *(Leave blank)*.

Block 2. Report Date. Full publication date including day, month, and year, if available (e.g. 1 Jan 88). Must cite at least the year.

Block 3. Type of Report and Dates Covered. State whether report is interim, final, etc. If applicable, enter inclusive report dates (e.g. 10 Jun 87 - 30 Jun 88).

Block 4. Title and Subtitle. A title is taken from the part of the report that provides the most meaningful and complete information. When a report is prepared in more than one volume, repeat the primary title, add volume number, and include subtitle for the specific volume. On classified documents enter the title classification in parentheses.

Block 5. Funding Numbers. To include contract and grant numbers; may include program element number(s), project number(s), task number(s), and work unit number(s). Use the following labels:

C	- Contract	PR	- Project
G	- Grant	TA	- Task
PE	- Program Element	WU	- Work Unit Accession No.

Block 6. Author(s). Name(s) of person(s) responsible for writing the report, performing the research, or credited with the content of the report. If editor or compiler, this should follow the name(s).

Block 7. Performing Organization Name(s) and Address(es). Self-explanatory.

Block 8. Performing Organization Report Number. Enter the unique alphanumeric report number(s) assigned by the organization performing the report.

Block 9. Sponsoring/Monitoring Agency Name(s) and Address(es). Self-explanatory.

Block 10. Sponsoring/Monitoring Agency Report Number. *(If known)*

Block 11. Supplementary Notes. Enter information not included elsewhere such as: Prepared in cooperation with...; Trans. of...; To be published in.... When a report is revised, include a statement whether the new report supersedes or supplements the older report.

Block 12a. Distribution/Availability Statement. Denotes public availability or limitations. Cite any availability to the public. Enter additional limitations or special markings in all capitals (e.g. NOFORN, REL, ITAR).

- **DOD** - See DoDD 5230.24, "Distribution Statements on Technical Documents."
- **DOE** - See authorities.
- **NASA** - See Handbook NHB 2200.2.
- **NTIS** - Leave blank.

Block 12b. Distribution Code.

- **DOD** - Leave blank.
- **DOE** - Enter DOE distribution categories from the Standard Distribution for Unclassified Scientific and Technical Reports.
- **NASA** - Leave blank.
- **NTIS** - Leave blank.

Block 13. Abstract. Include a brief *(Maximum 200 words)* factual summary of the most significant information contained in the report.

Block 14. Subject Terms. Keywords or phrases identifying major subjects in the report.

Block 15. Number of Pages. Enter the total number of pages.

Block 16. Price Code. Enter appropriate price code *(NTIS only)*.

Blocks 17. - 19. Security Classifications. Self-explanatory. Enter U.S. Security Classification in accordance with U.S. Security Regulations (i.e., UNCLASSIFIED). If form contains classified information, stamp classification on the top and bottom of the page.

Block 20. Limitation of Abstract. This block must be completed to assign a limitation to the abstract. Enter either UL (unlimited) or SAR (same as report). An entry in this block is necessary if the abstract is to be limited. If blank, the abstract is assumed to be unlimited.

Table of Contents

List of Figures

List of Figures (concluded)

Section 1
Executive Summary

The Optoelectronic Technology Consortium was established to demonstrate the producibility of high-density/high-data-rate optoelectronic components for military and commercial applications, including the interconnection of avionics or shipboard processing nodes, mainframe computer cabinets, workstation clusters, and telecommunication switch cabinets. Specifically, the goal was to develop an affordable optoelectronic transmitter and receiver modules with an aggregate data transfer rate of 16 Gbit/s with a line bit error rate (BER) $<10^{-15}$. The overall program consisted of a baseline approach as well as several alternative approaches. The baseline approach involved the use of parallel fiber ribbon cable as the transmission medium, with a vertical-cavity surface-emitting laser (VCSEL)-array transmitter and a GaAs-based integrated photodetector/ amplifier array receiver module. As alternative transmitters offering potentially higher temperature operation and reliability, AlGaAs-based waveguide modulator arrays were developed by Honeywell under the program. Another alternative was the development of board-level polymer waveguides for shorter distance, higher interconnect density applications within a box or cabinet. As the program progressed, however, VCSELs were found to be more promising for high-temperature applications, so the waveguide modulator task was deemphasized, while Honeywell assumed the task of providing a second source of VCSELs.

Therefore, our tasks, to be described in this report, included (1) the development of a four-element AlGaAs waveguide modulator array, (2) its associated optical and electrical packaging, (3) an experiment to evaluate the performance limits and alignment tolerances of board-to-board polymer waveguide optical interconnects, and (4) the development of a VCSEL array capability.

Each packaged AlGaAs modulator array consists of a single-mode fiber input coupled to one waveguide input, which is then split on-chip into four Mach-Zehnder interferometric modulators with a 1×8 fanout circuit (two arms for each modulator). The arms of each modulator are recombined into a single waveguide with 2×1 combiner elements, and then the four output waveguides are coupled to four multimode fibers. We compared conventional splitters and combiners (i.e., a waveguide very gradually splits into two) with multimode interference splitter and combiner structures and found that the latter were the lowest loss approach, in addition to being more compact. We also found that a p-i-n epitaxial waveguide structure provided a factor of 2 improvement in required modulator drive voltage efficiency over an undoped structure, with only a slight penalty in optical loss. We showed that extinction ratios in excess of 10 dB, a 20–25 V-mm drive voltage-length product, and performance to 143°C range of operation can be achieved with little change in maximum output power or extinction ratio. However, we also found the devices to be quite sensitive to the lateral dimensions of the waveguide as well as to stress induced by device processing or packaging.

We also demonstrated packaging techniques that allowed single-mode polarization-maintaining fiber to be coupled to the input of the AlGaAs waveguide with only 1-dB variation in coupling efficiency up to 110°C. However, the packaging is very labor intensive, the pigtailed high-power input lasers are very expensive, and the stress induced by the packaging can have a dramatic effect on modulator performance.

We demonstrated that low-loss polymer waveguides can be fabricated on standard board materials with reasonable optical loss, and that a single expanded-beam connector can provide a high density of board-to-board connections (i.e., up to 60 channels per 3-mm lens pair). The required board-to-board alignment tolerances were found to be +0.37/–0.25 mm and +0.19/–0.15 deg, which are consistent with typical fabrication tolerances for boards and chassis.

In the VCSEL area, we migrated the Honeywell VCSEL process from one designed to be more compatible with monolithic integration toward an approach similar to that taken by AT&T under this program (i.e., a planar process that uses proton implantation to provide current confinement). We were able to reduce the resistance of our devices by improving the p-ohmic contact. We also incorporated higher Al composition cladding layers in the cavity, which allowed us to increase the temperature range of operation.

Our work under this program has demonstrated the feasibility of fabricating and packaging a transmitter array consisting of waveguide modulators based on the electro-optic effect. These transmitters provide good performance to very high temperatures (i.e., >140°C). Although reliability testing has not been carried out, the fact that the transmitters are reverse-biased leads us to believe that they will have good reliability. However, these devices require very careful attention to the details of the fabrication and the stress induced in fabrication or packaging, and they are quite large. All of these factors lead to a relatively high cost. Based on our experience in both waveguide modulators and VCSELs, as well as the experience at AT&T, we are confident that VCSELs are a lower cost approach, at least for applications in the 0°–70°C temperature range, and will be the emitter of choice for commercial applications. Although high-temperature operation has already been demonstrated, the reliability of the devices at temperatures up to +125°C remains to be evaluated.

We have also addressed several critical issues in the practical realization of polymer-waveguide-based board-level interconnects. These include their compatibility with standard board assembly processes, the high connection density that can be achieved in the expanded-beam connectors, and their tolerance to misalignment. Although these principles have been demonstrated, further engineering work is required to develop a production-ready fabrication and assembly process.

Section 2
Introduction

The Optoelectronic Technology Consortium was established to position U.S. industry as the world leader in optical interconnect technology by developing, fabricating, integrating, and demonstrating the producibility of optoelectronic components for high-density/high-data-rate processors and accelerating the insertion of this technology into military and commercial applications. This objective was accomplished by a program focused in three areas:

- Demonstrated Performance—OETC demonstrated an aggregate data transfer rate of 16 Gbit/s between single transmitter and receiver packages.
- Accelerated Development—By collaborating during the precompetitive technology development stage, OETC advanced the development of optical components and produced links for testbed demonstration.
- Producibility—OETC's technology achieved this performance by using components that are affordable and reliable, with a line BER $<10^{-15}$ and MTTF $>10^{6}$ hr.

Under the OETC program, Honeywell developed packaged AlGaAs arrays of waveguide modulators and polymer-based, high-density, parallel optical backplane technology compatible with low-cost manufacturing. The scope of the program was modified such that the number of packaged waveguide modulator arrays to be fabricated under the program was reduced and efforts were initiated in the development of vertical-cavity surface-emitting lasers (VCSELs).

The packaged AlGaAs modulator arrays consist of a single fiber input, a 1×4 fanout circuit, four waveguide modulators, and four fiber outputs, all mounted on a ceramic header. The primary benefit of this approach is enhanced system reliability, particularly at high temperatures. Combined with the demonstrated high density of these devices when fabricated in arrays, this allows the development of compact and reliable transmitter components.

The objective of the polyimide backplane development effort was to demonstrate a practical high-density (>20 lines or channels per mm) parallel optical backplane facilitating (bandwidth × length/power) interconnect figures of merit between one and two orders of magnitude greater than would be attainable with state-of-the-art electrical interconnects. The effort addressed both development of an ultimately manufacturable and environmentally tolerant optical backplane and the optical interface concepts required for practical board-to-backplane optical connection. The key functionalities and compatibility with standard multiboard assembly practices were demonstrated in a laboratory evaluation system.

Section 3
Technical Approach

3.1 AlGaAs Modulator Array Development

The decision to include waveguide modulators in the OETC project as an alternative transmitter source was due to the requirement that the link be applicable to both defense and commercial applications. Project members felt that the modulators were more likely than lasers to operate over the full military specification range. They were also expected to be more reliable because they are reverse-biased devices. During the program, dramatic improvements were seen in the performance of VCSELs as a function of temperature, providing confidence that they would operate satisfactorily under commercial conditions and optimism that they could also meet the needs of military environments. Therefore, part way through the program, a decision was made to reduce the modulator arrays level of effort and to begin developing Honeywell capability in VCSELs. The approach to modulator development will be described here, and the VCSEL effort will be described later.

The philosophy for implementation of modulator-based parallel transmitters was that the arrays of modulators would be located in the demanding environment of a processor board of a system. The continuous-wave (CW) light source feeding the modulators would be located remotely in an environmentally controlled location. To minimize the laser resources and the number of fibers that must be pigtailed to the modulators, as well as maximize real estate on the board, the approach taken was to use one laser to feed several modulators and to do the splitting of the input laser light into several channels on the same chip as the modulators. The number of modulators to be fed by each laser is determined by a tradeoff of the amount of power that can be delivered to each modulator and the loss budget, as well as the cost of the laser providing a given amount of power and the cost of coupling a single-mode, polarization-maintaining fiber to the input of the waveguide. The highest power laser that one could obtain at a reasonable cost (about $4,000 pigtailed) outputs 100 mW. Taking into account all of the losses (as will be described in the results), the largest array size that could be fed by a single laser was determined to be 4. The approach taken in design and fabrication of the modulator array chip itself is to have a chip with one single-mode input waveguide accepting a CW optical input from a single-mode, polarization-maintaining fiber, in turn attached to the output of a laser diode. The input waveguide splits into eight waveguides, forming the arms of four separate Mach-Zehnder interferometers. The two arms of each modulator are recombined into one output waveguide or four waveguides total, which are coupled into four multimode fibers at the output side of the chip. Translation of the electrical signal to an optical format in the modulator relies primarily on the linear electro-optic effect. An optical signal propagating through a waveguide suffers a phase delay that depends on the effective refractive index of the guided mode. By appropriate application of an electric field, the phase of the guided wave can be altered. By combining the outputs of two waveguides, each suffering a different degree of phase retardation with applied voltage, amplitude modulation results. Initially, the waveguides were designed to be nominally undoped with Schottky contacts made to the top surface. However, it was subsequently determined that a p-i-n doped structure would give much improved voltage-length products as well as more reproducible results at very little cost in terms of increased propagation loss. Rather

than use gradual splitters and combiners, we chose to use an alternative design methodology incorporating waveguide imaging. In such as design, a single-mode input waveguide is connected to a laterally multimoded waveguide section, which is in turn connected to a multiplicity of single-moded output waveguides on a specific output grid spacing. For the correct dimensions of the multimode section, multiple images of the input waveguide can be formed on the output image plane. The multiple images result from lateral mode interference, so we refer to these components as multimode interference (MMI) splitters and combiners. The advantage of this approach to the splitters is the reduced real estate required.

The epitaxial layers forming the waveguide are deposited by organometallic vapor phase-epitaxy (OMVPE) on 3-in.-dia. semi-insulating (100) GaAs substrates grown by the liquid-encapsulated Czochralski (LEC) method. The structure is grown at a pressure of 200 mbar and at a substrate temperature of 760°C in an AIX 200/4 reactor. The structure is illustrated in Figure 3-1. A 0.3-μm GaAs buffer layer is deposited first, followed by a 10-period 10-nm AlAs/10-nm GaAs superlattice. The intent of both the GaAs and superlattice buffer layers is to provide a very smooth surface morphology to minimize optical scattering loss. The waveguide layers are grown next, starting with the $Al_{0.3}Ga_{0.7}As$ bottom clad layer with a total thickness of 3 μm. In the case where the structure is doped, the first 1.6-μm thickness is doped n-type to a level of $1 \times 10^{18}/cm^3$, the next 1-μm thickness is doped n-type to a level of $5 \times 10^{17}/cm^3$, and the last 0.4-μm thickness of the clad located next to the core is doped n^- ($<1 \times 10^{16}/cm^3$). The core layer consists of 1 μm of $Al_{0.26}Ga_{0.74}As$ with the bottom 0.5 μm doped n^- and the top 0.5 μm doped p^- (both $<1 \times 10^{16}/cm^3$). The top clad layer consists of 1 μm of $Al_{0.30}Ga_{0.70}As$ with the first 0.4 μm doped p^- and the top 0.6 μm doped p-type to a level of $5 \times 10^{17}/cm^3$. The last layer of the structure is a 20-nm p^+ GaAs capping layer that protects the surface from oxidation and assists in good ohmic

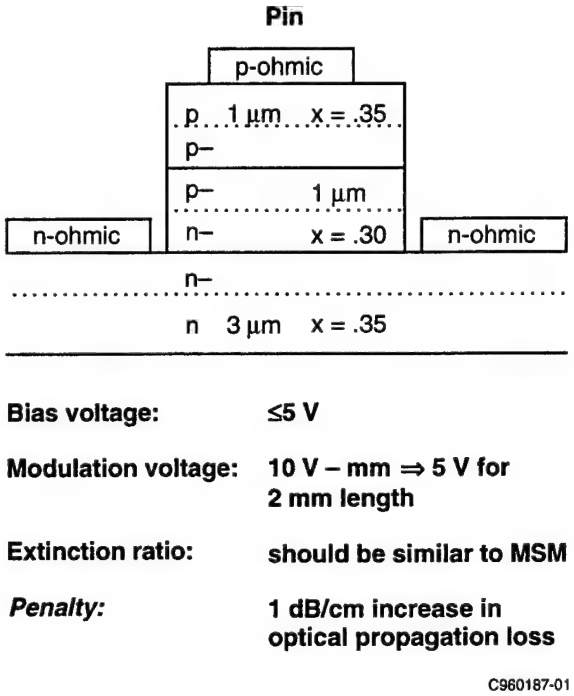

Figure 3-1. Tradeoff: MSM vs. Pin Modulator Design

contact formation. The sources used include trimethylgallium, trimethylaluminum, 100% arsine, diethylzinc as the p-type dopant and 50-ppm diethyltellurium in hydrogen as the n-type dopant. The n^- and p^- doping levels are achieved with no intentional doping but rather by controlling the V/III ratio (i.e., the ratio of arsine to trimethylgallium and trimethylaluminum). The V/III ratio was approximately 70 for the doped and p^- clad layers, 85 for the n^- clad layer, 64 for the n^- core layer, and 58 for the p^- core layer.

The waveguide structures are defined using chlorine-based reactive ion etching. The mask dimensions defining the single-mode guides were 2.0 μm. The structures were etched down through the core layer. This provides a large index difference that allows more compact routing of guides. TiAu metal is deposited and patterned to form both the top and bottom electrodes. These electrodes are connected to bond pads regularly spaced at the side of the chip by air bridges. This is preferable to the use of polyimide planarization, as undesirable polarization-related effects can arise from the stress associated with the polyimide.

3.2 AlGaAs Modulator Array Package Design and Fabrication

The package must support the optical, electrical, and mechanical functions of the modulator transmitter module. The mechanical design of the package must provide stable location of the input and output fibers with respect to the modulator chip, whereas the electrical design must accommodate the modulator, bias network, and driver array. The materials selected must be compatible with operation over the projected operating temperature range while allowing adequate electrical performance.

The fiber used in the packaging has a profound influence on packaged device loss. Keeping the modulator parameters fixed, we considered a range of commercially available single-mode polarization-maintaining fibers. The fibers were evaluated by measuring the mode dimensions and using the measurements in combination with those of the waveguide modulator. Our optimization revealed that the most suitable commercially available fiber was a D-shaped design supplied by Andrew Corporation. This fiber has the desirable feature that the refractive index difference between core and cladding is large, resulting in a small mode size. In the OETC testbed demonstration for which this modulator was designed, the interconnect medium is multimode fiber of 62.5-μm core diameter and 125-μm outside diameter. The fibers are assembled into an array on 140-μm centers. Therefore, this fiber was the automatic choice for the fiber coupled to the output side of the modulator array. The same silicon V-groove assembly used in the MAC connector and for coupling fiber to the VCSEL and photodetector arrays was used to hold the four output fibers at a 140-μm pitch and allowed the simultaneous alignment of all four fibers to the modulator array output waveguides.

Having selected the optical fibers for our package, we designed a substrate to optimally locate all optical components over as broad a temperature range as possible. The mechanical arrangement devised for ensuring stable single-mode fiber-to-waveguide alignment is shown in Figure 3-2a. The modulator is mounted on an alumina submount. Alumina has a coefficient of thermal expansion well matched to GaAs, minimizing temperature-induced strain on the modulator while also ensuring that the fiber does not change height with respect to the upper surface of the modulator. The Si V-groove assembly is located on the same plane as the modulator chip. Figure 3-2b shows the entire optical subassembly.

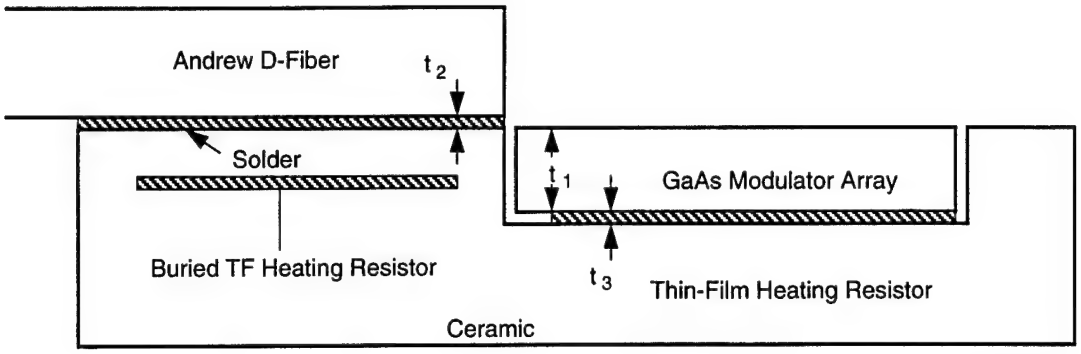

Figure 3-2a. Single-Mode Pigtail Assembly Technique

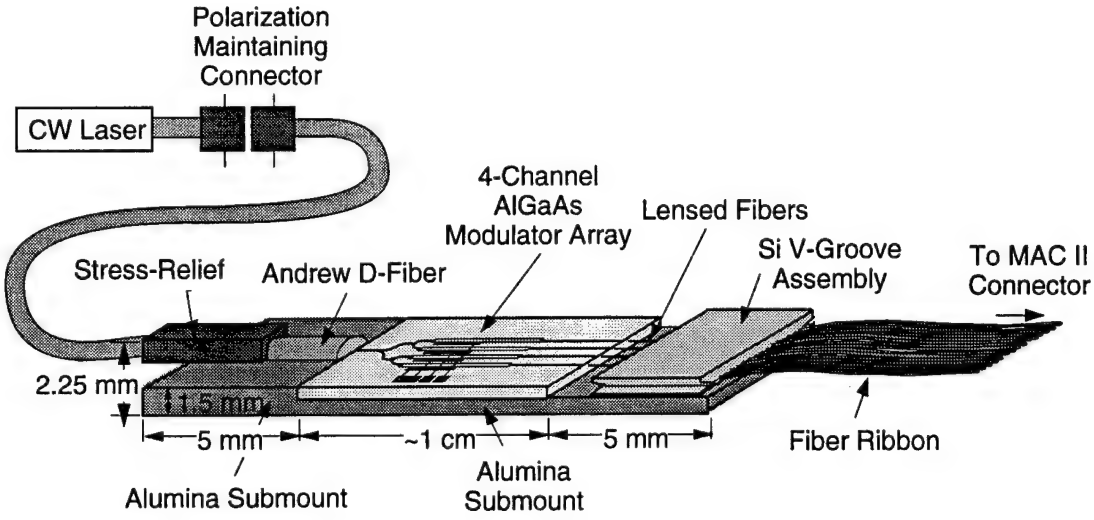

- Requirement: deliver minimum –10 dBm to each fiber in fiber array (3 dB system margin)
- Assembled submount dimensions: 20 mm x 5 mm x 2.25 mm
- Package designed for operation over full military spec range (–55 to 125°C)

C960187-02

Figure 3-2b. Waveguide Modulator Array Submount

The modulator driver array was fabricated using a standard GaAs E/D MESFET foundry process developed by Triquint. Unpackaged die were supplied by the foundry and were then tested to verify correct operation before being included in the package. The bias networks were fabricated using a thick-film multilayer substrate in which linewidths of 0.010 in. and dielectric layer thicknesses of 0.010 in. aim to provide an impedance of approximately 50 Ω. Figure 3-3 shows the layout of the bias networks. The selection of filter elements and values was based on simulations done at Martin Marietta.

Due to the potential sensitivity of the optical alignment to mechanical disturbance before completion of the modulator, all electrical packaging was performed first. Figure 3-4 shows a

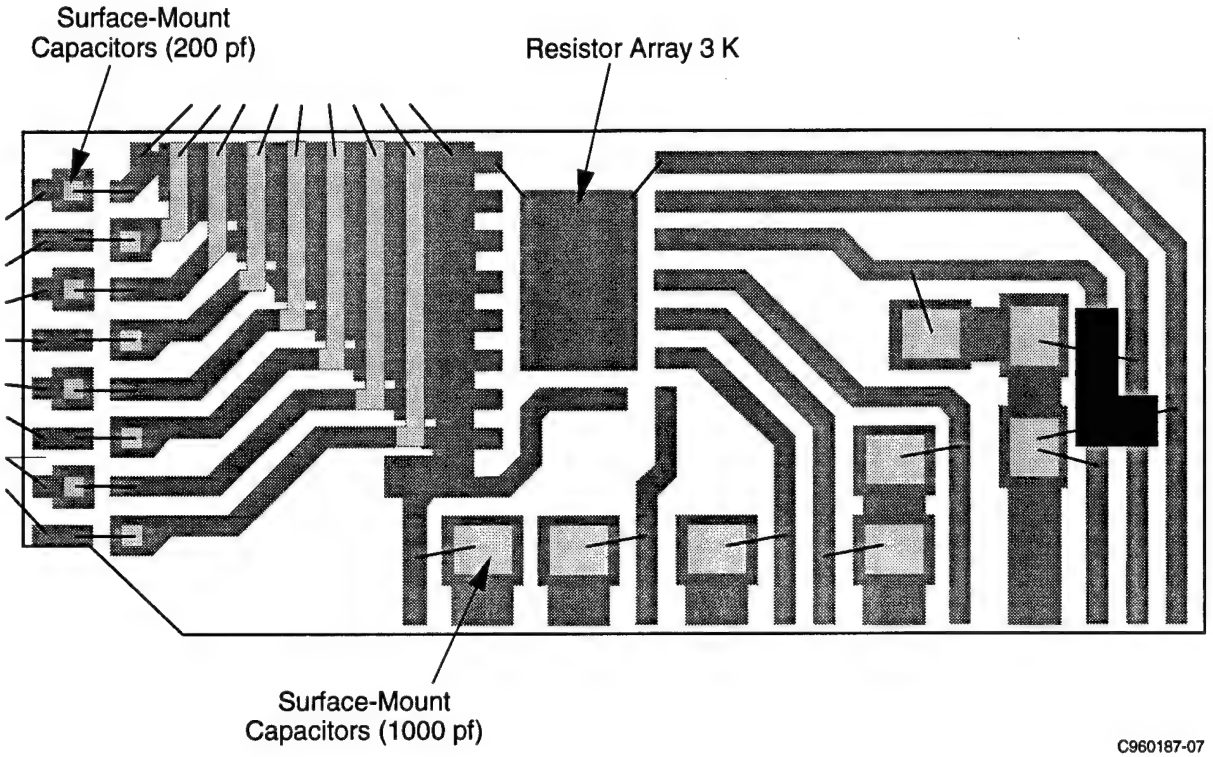

Figure 3-3. AlGaAs Waveguide Modulator Array at 830-nm Wavelength

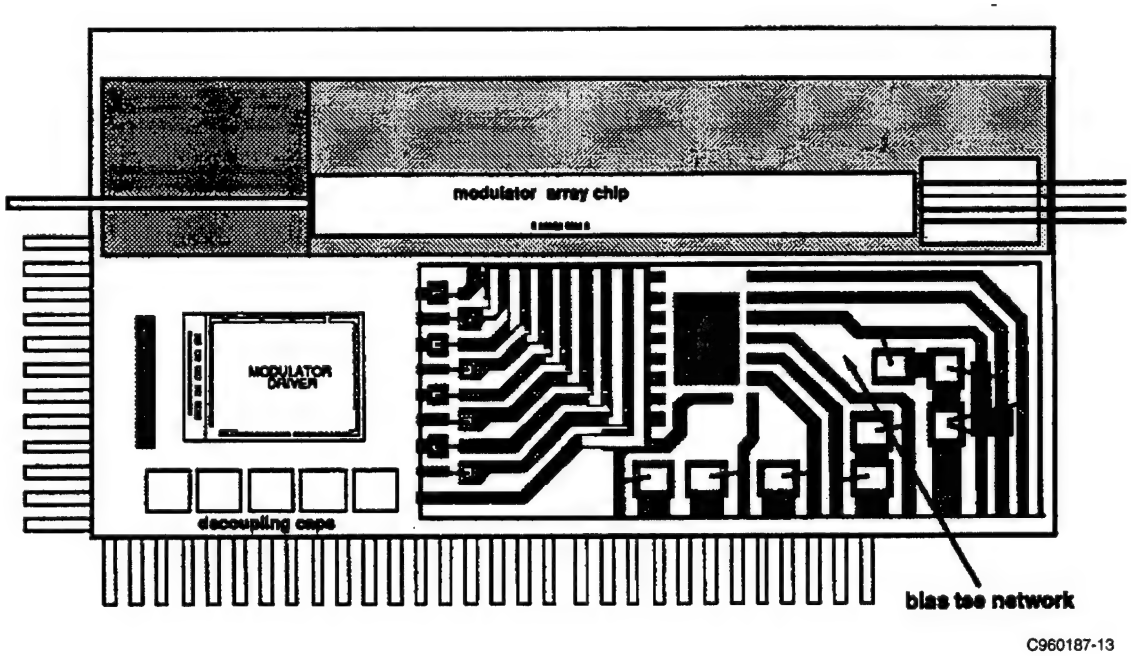

Figure 3-4. A Schematic Diagram of the Modulator Package Incorporating the Modulator Array, Single-Mode Fiber Input, Multimode Fiber Outputs, Modulator Driver Chip and Bias Tee Network

schematic of the total transmitter package. The optical subassembly, the bias tee, and the driver chip are all bonded directly to the heat spreader. The modulator is attached to the alumina submount using a thermoplastic preform. Thermoplastics are attractive materials for robust packages, as long-term creep associated with solders is avoided and potential instabilities and outgassing difficulties with epoxies do not occur. The bias network and the driver circuit were added to the heat spreader using similar techniques, after which electrical interconnects were made by wirebonding. The heat spreader is AlN with a metal layer on top. The metallized heat spreader is also used as a ground plane for electrical reference. The heat spreader is bonded to the lead frame outer package. Part of the alumina lead frame sidewall is cut out to provide access for the input and output to the optical subassembly.

The single-mode input fiber was mounted on a ceramic block with a sawn slot to ease handling. The ceramic block was then manipulated to align the fiber with the waveguide. Epoxy was used in this case to affix the fiber, with care taken in the selection of the epoxy to ensure minimum shrinkage. During the single-mode input alignment, a gradient-index (GRIN) lens was used to image the output of a channel waveguide onto a detector, allowing active optimization of the alignment. At the output of the modulator array, lensed fibers supplied by Spectran Corporation were mounted in a silicon V-groove array and capped with a second V-groove array. This array was aligned with respect to the modulator array and again assembled using epoxy. Active alignment was also employed for this step to minimize loss incurred by misalignment. The CW optical supply beam was provided by a 100-mW semiconductor laser produced by Spectra Diode, Inc., and was pigtailed and equipped with a connector by Seastar, Inc., using the same polarization-maintaining single-mode fiber used for the input pigtailing to eliminate additional losses due to the mode-mismatch at the connector.

Measurements of the tolerance to misalignment and temperature were made and compared to calculations of theoretically possible results. Measurements were performed after both fabrication of the optical subassembly and assembly of the total transmitter module. The various interfaces were analyzed both experimentally and theoretically to understand the distribution of optical loss.

3.3 Polymer Backplane Experiment

This experiment lays the groundwork for extension of the parallel-fiber-based links to the formation of parallel links at the board level. The effort uses polymeric waveguides to implement high-density routing components and interconnect structures. The task encompasses the demonstration of both the passive waveguide structures themselves, using commonly encountered backplane materials, and the interfacing of waveguides from one board to another, for example, as from a daughterboard to a motherboard in a typical backplane-based system.

The overriding philosophy of this work is to make the polymer waveguide fabrication and connector design compatible with standard board fabrication and installation. To this end, our goals were to fabricate optical waveguides on board materials widely used in the electronics industry and to develop a board-to-board connector with alignment tolerances similar to those currently specified for boards.

Our baseline material choice is a glass/polyimide laminate system. Materials commonly encountered in avionics systems for both boards and backplanes are glass/epoxy for lower temperature applications (up to 100°C) and glass/polyimide for higher temperature operation (up to 250°C continuous operation) at approximately twice the cost. More esoteric materials such as PTFE (Teflon-based) backplanes are generally used only when high-frequency electrical signals (hundreds of megahertz) are used, and may be four times as expensive as glass/polyimide while severely restricting the number of layers that may be incorporated into a multilayer board. A significant advantage of optics is that multigigahertz signals may be routed using polymer waveguides on the lower cost polyimide/glass substrates. Our baseline material choice is glass/polyimide. We integrate our polymer waveguides into the board using a standard process (i.e., by lamination into a multilayer stack with 100- to 200-psi pressure and up to 250°C. The use of a planarizing polymer to smooth the relatively rough surface of the board is being investigated.

The target dimensions of the waveguide are a height of at least 20 μm and comparable widths. The resulting waveguide densities, up to 50 per millimeter, approach an order-of-magnitude higher density than can be practically attained using standard optical fiber. After some experimentation, the standard for the polymer materials became BCB as the bottom clad layer, which also serves to planarize the board surface. The core consists of Ultem, a product of General Electric. The top clad also consists of BCB. The core is patterned using oxygen reactive ion etching.

The baseline approach that has been identified for interfacing the optical backplane waveguides to waveguides on the daughterboards is to use expanded beam connectors with multiple channels sharing a given connector. Each channel is associated with a particular angle of propagation of the expanded beam with respect to the optical axis. Appropriate choice of optical components will allow negligible crosstalk while allowing fractions of a millimeter positional alignment. Despite the relaxed tolerances at the board-to-backplane interface, each channel must be located accurately with respect to the GRIN-lens-based connector. This is achieved by photolithographically patterning the spot where the lens is to be placed at the same time the waveguide is patterned. The lens can then be dropped into place and is automatically aligned with respect to the waveguides.

Figure 3-5 illustrates the experiment performed to evaluate connector performance limits. To evaluate the crosstalk characteristics of the GRIN lens used for the connector, a set of input guides and a separate set of output guides were interconnected using a conjugate pair of GRIN lenses. The waveguide end faces are located at the focal plane of the lenses. The interface between the two lenses is therefore an expanded beam. In a practical board-to-backplane connector, the 90-deg directional change would be effected by a micro-optical prism mounted between the board and backplane lens fixtures.

Figure 3-6 illustrates the setup used to measure the alignment tolerances of the board-to-backplane connector. Each of the boards was mounted on a micropositioner stage. Light was input into the first waveguide, and the optical output of the waveguide on the second board was measured as a function of the position and angle of the first board with respect to the second.

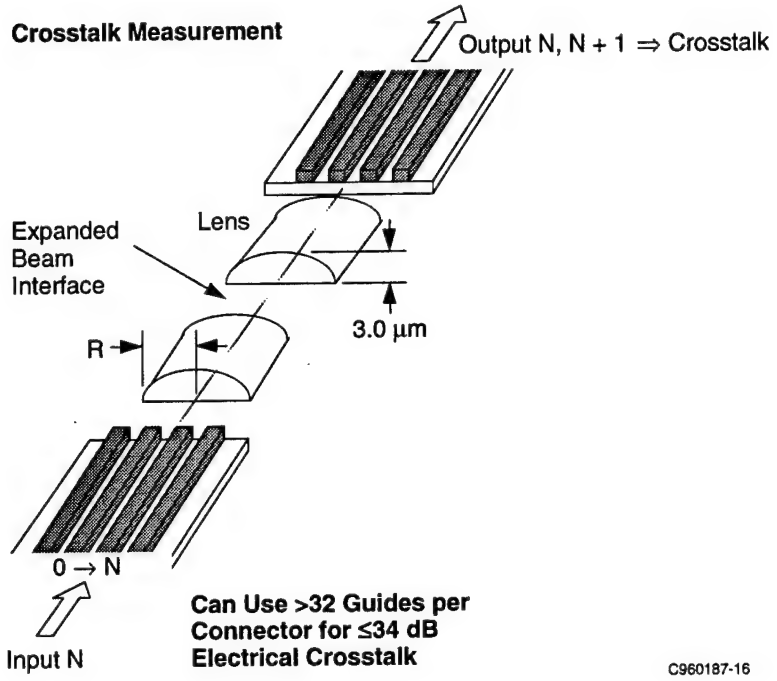

Figure 3-5. Crosstalk Evaluation of Board-to-Backplane Connector

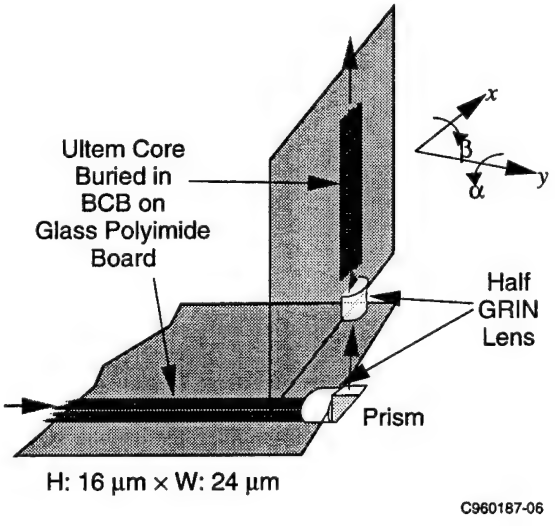

Figure 3-6. Schematic of Polymer Backplane Experiment

3.4 VCSEL Array Development

Honeywell has previously developed a VCSEL structure for integration with photodetectors and Field Effect Transistors (FETs) on semi-insulating substrates that differed in many respects from the structure developed by AT&T and applied to the fabrication of OETC arrays. The two structures are illustrated in Figure 3-7. The baseline AT&T OETC approach deposits layers on a

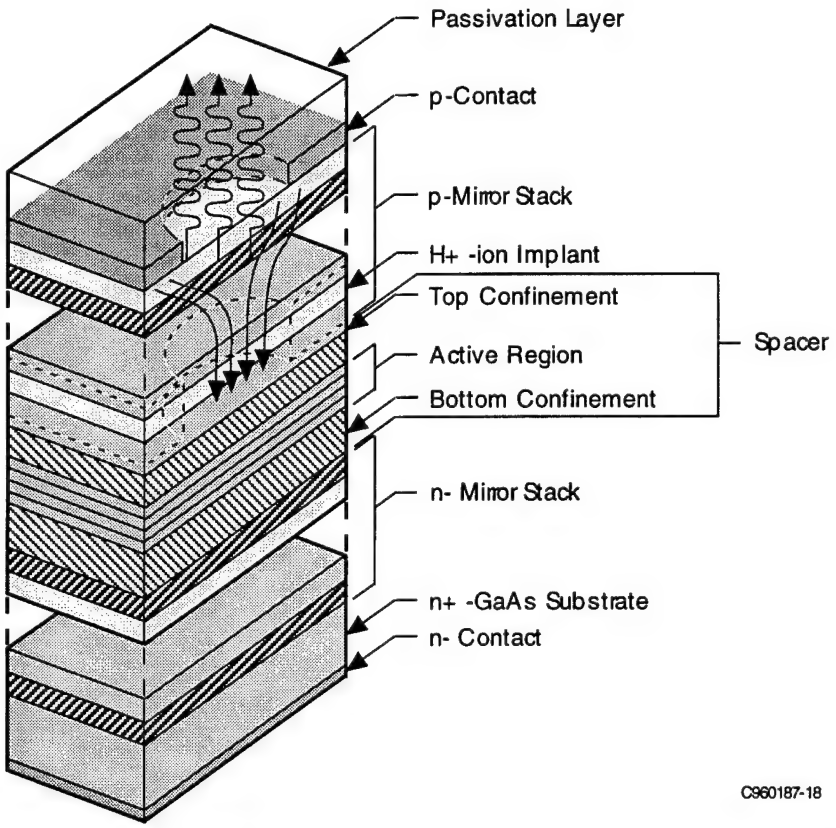

Figure 3-7a. Schematic of Top-Surface-Emitting Vertical-Cavity Laser

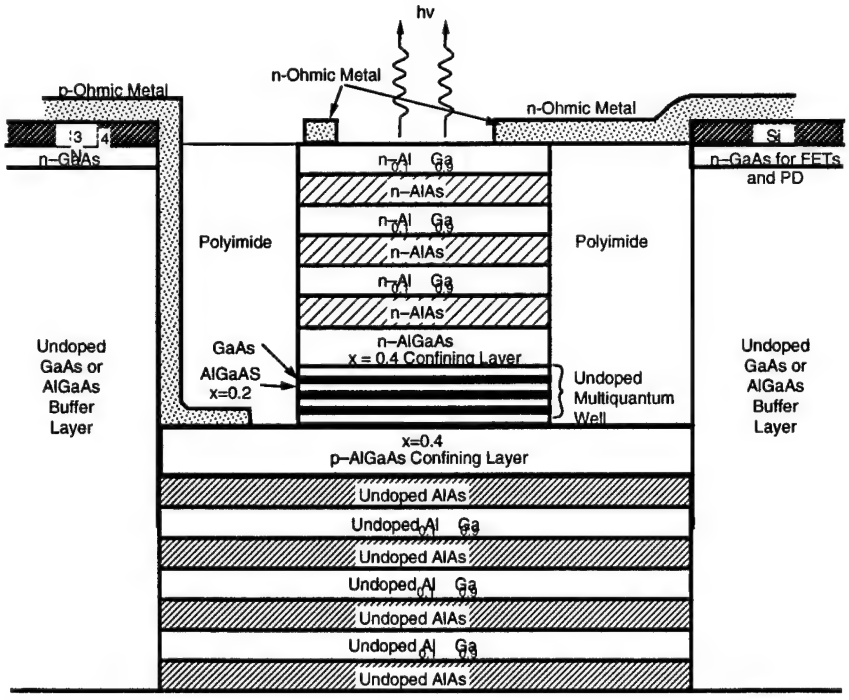

- Separate epitaxial layers for laser and electrical circuit allow independent optimization
- Approach adaptable to a variety of devices (Laser, LED, SEED) and circuit technologies (MESFET, HEMT, C-HIGFET)

Figure 3-7b. Approach to Integration of VCSELs with MESFET

doped substrate. The cavity is sandwiched between two epitaxial semiconductor mirrors, and the cavity thickness (in the vertical direction) corresponds to one wavelength. The lateral dimensions of the laser cavity are defined by a proton implantation. A broad-area contact is deposited on the substrate side of the wafer, and individual contacts are patterned on the top side. In contrast, our previous Honeywell structure was designed to accommodate a semi-insulating substrate, so that one cannot make a broad-area contact on the substrate side. Therefore, we include in our cavity a thicker doped n-layer that can be contacted from the top side. This is accomplished by using reactive ion etching to etch down to the contact layer, which also simultaneously defines the lateral extent of the laser cavity. A metal contact is made to this contact layer. The total cavity thickness, including this contact layer, corresponds to three wavelengths. The other metal contact is made to the top surface of the original epitaxial growth.

As we were not constrained by the requirement to integrate the VCSELs with FETs, we decided to migrate toward the proton-implanted structure because it is simpler and is a planar process. As an intermediate step, we fabricated a device that was deposited on a doped substrate and had a broad-area contact on the back side. The cavity also corresponded to one-wavelength thickness; however, we still used dry etching to define the cavity. In addition, we modified the design of the cavity with the intent of improving the performance as a function of temperature. This involved increasing the aluminum content of the cladding layers in the cavity. In addition, experiments with the doping at the top surface were carried out to understand the contribution of the ohmic resistance to total device resistance. This involved varying the amount of p-dopant flow during deposition of the layers in the top mirror period. Testing included measurement of light output versus current and current versus voltage at a range of temperatures.

Section 4
Results

4.1 AlGaAs Modulator Array Development

Desired characteristics for the waveguide modulator array include a small voltage-length product to limit both the applied voltage and the chip real estate required and to achieve a low optical propagation loss, a high extinction ratio, a breakdown voltage comfortably above the required drive voltages, stable operation over the required temperature range, as well as good uniformity in performance within and between arrays. This section illustrates these performance characteristics. We will examine the tradeoffs between the use of an undoped or a p-i-n modulator structure as well as the use of a conventional small-angle splitter versus a multimode interference splitter.

4.1.1 Passive Optical Propagation Loss

Optical propagation loss was measured by cutback measurements (i.e., by measuring the optical throughput of a waveguide cleaved into segments of different lengths). Measurements made on nominally undoped unetched epitaxial waveguide layers (i.e., planar waveguides) indicated a propagation loss of 0.3 dB/cm. This is quite acceptable and is indicative of the material's optical quality. This loss number is typically degraded by etching individual waveguides due to the resulting sidewall roughness. For 2-μm-wide guides defined by reactive ion etching, the propagation loss of nominally undoped guides was 2 dB/cm. This was increased to 3 dB/cm for 2-μm wide p-i-n doped guides (described in Section 3, Technical Approach). This increase in loss for the doped structure can be tolerated if there is a reasonable payoff in other performance characteristics. We believe this is true as will be demonstrated below.

4.1.2 Voltage-Length Product Comparison of Undoped and p-i-n Mach-Zehnder Modulators

Figures 4-1a and 4-1b illustrate the light versus voltage (L-V) performance achieved in undoped and p-i-n doped Mach-Zehnder modulators, respectively. Figure 4-1a shows the L-V characteristics when the two arms of the modulator are reverse-biased independently. VL (voltage-length product for π phase change) and ER (extinction or on-off ratio) for this 1-cm-long device are measured to range from 5.3 to 5.6 V-cm and 8.2 to 9.2 dB. The plots labeled N and S correspond to reverse bias applied to each of the arms of the Mach-Zehnder independently. A complementary driver would only need to provide half this voltage to each electrode to achieve the same change in transmission.

The transmission curve of Figure 4-1b was obtained from a p-i-n doped Mach-Zehnder by driving only one of the electrodes, similar to the case in Figure 4-1a. At room temperature, the voltage length product of the modulator is 2.4 V-cm, because the electrode length for this sample was 4 mm. We have verified that with optical input levels as high as 30 mW, no variation in the transfer function occurs. The extinction ratio is 10 dB. This can vary from approximately 6 dB to as high as 23 dB, with polarization effects appearing to be the limiting value. Many of the polarization rotation effects, in turn, appear to be related to stress induced by metal or dielectric layers deposited during device fabrication.

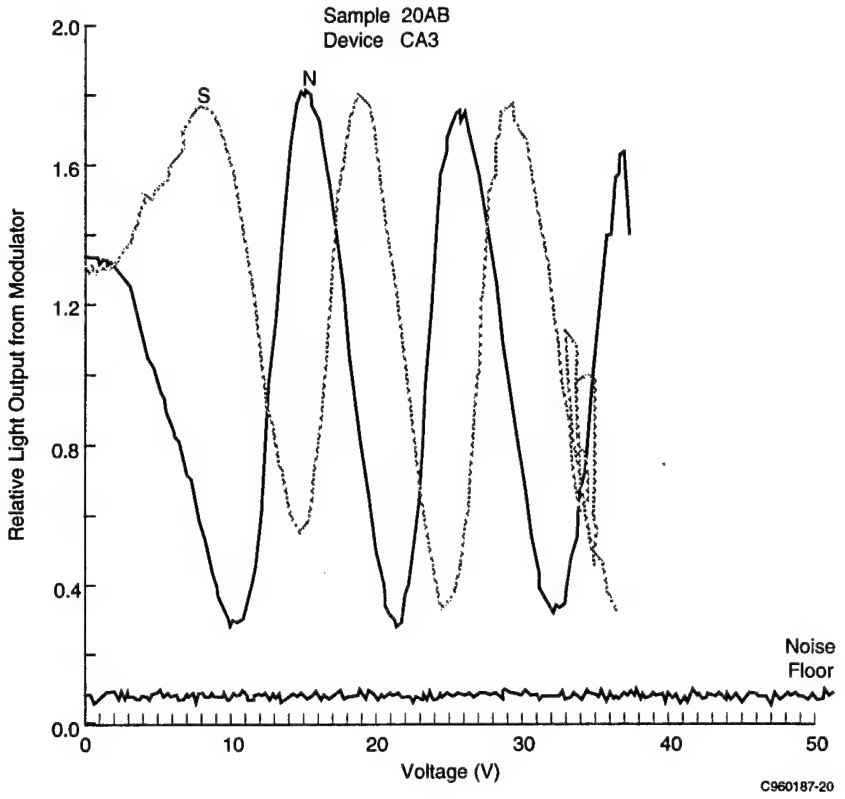

Figure 4-1a. Light Output vs. Applied Voltage for the Two Arms of a Mach-Zehnder Interferometer (The plots labeled N and S Correspond to Reverse Bias Applied to Each of the Arms of the Mach-Zehnder Independently.)

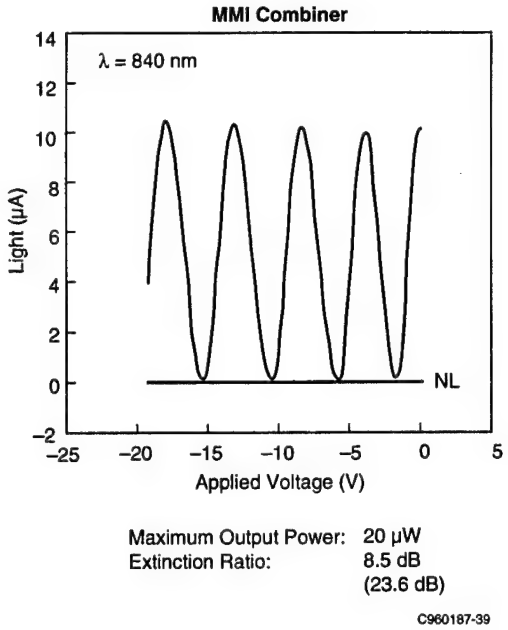

Figure 4-1b. Measured Mach-Zehnder DC Characteristics

4.1.3 Performance of Conventional vs. Multimode Interference Splitters

Conventional splitter designs place stringent demands on processing as the two new guides separate at a very small angle from the original guide. One is therefore forced to etch a very sharp apex. Normal photolithography would tend to smooth this apex, resulting in additional loss. An alternative approach is to incorporate multimode interference effects in the design of a splitter. The splitter design and its incorporation in and application to a four-element modulator array is illustrated schematically in Figure 4-2. The splitter consists of a single-mode waveguide region that abruptly changes to a multimode guide and then abruptly into several single-mode guides at the output. The length and width of the multimode region determine the number and spacing of the output channels. This splitter design approach is better suited to the deeply etched fabrication process already developed at Honeywell in that all of the corners are 90-deg angles, rather than the very small angles (1 deg) required by the conventional splitter. Preliminary data for the one to eight splitter (as illustrated in Figure 4-2) is given in Figure 4-3. The curves marked "baseline, +δL, and –δL" refer to the multimode interference designs and indicate the baseline length for the splitter region, as well as lengths larger and smaller than baseline by 20 μm. The curves marked ROC refer to the conventional splitter designs with the radius of curvature (ROC) indicated. Figure 4-3a shows a very good uniformity of throughput lightwave power (initial results give a worst-case channel-to-channel difference of 1–2 dB), and Figure 4-3b indicates an excess insertion loss that is essentially independent of the number of output channels (4.4 ± 1.5 dB per device for the baseline design, exclusive of the intrinsic fanout loss). Even lower excess insertion loss (3 dB) is measured for the "–δL" case, perhaps indicating that the finished dimensions of the "–δL" multimode interference splitter were better matched to the wavelength of the input light. The data shown in Figure 4-3 for the conventionally designed 1×N splitters based on cascaded 1×2s indicates that the insertion loss scales as the number of 1×2s in the path decreases, with typical excess losses of about 4 dB per 1×2. In addition, the uniformity of the output light from the channels in an array is much inferior to that for the MMI splitter.

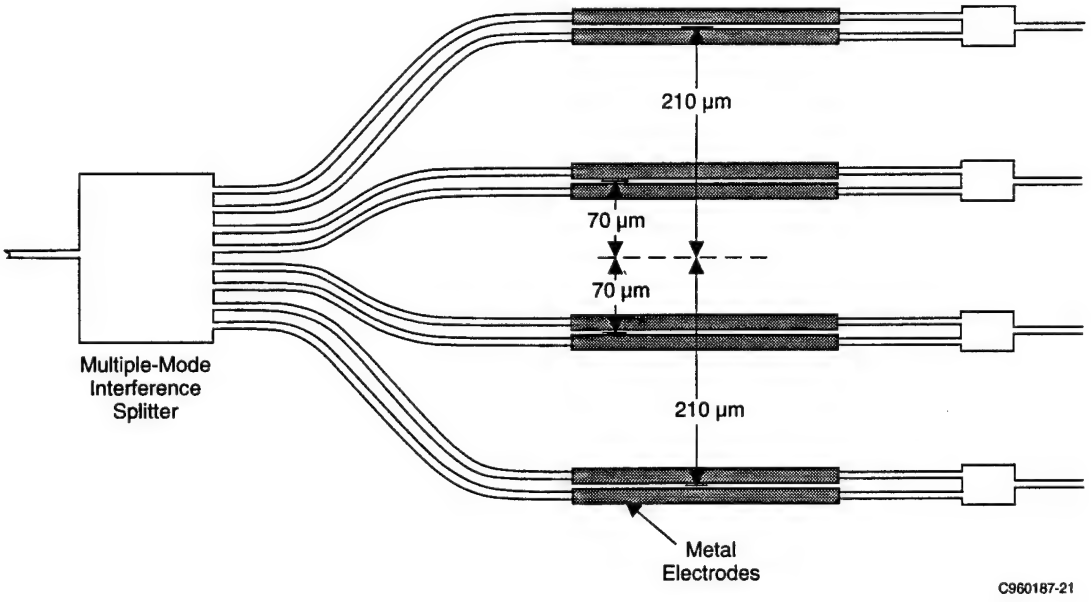

Figure 4-2. New Baseline Design for a Four-Element Modulator Array

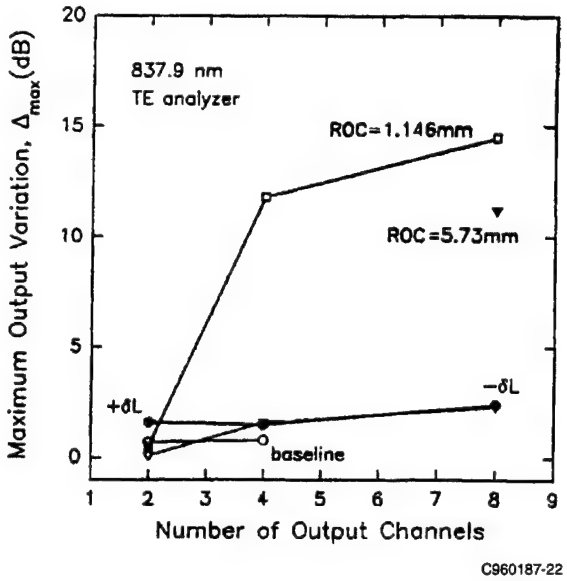

Figure 4-3a. Sample 55B—Splitter Results

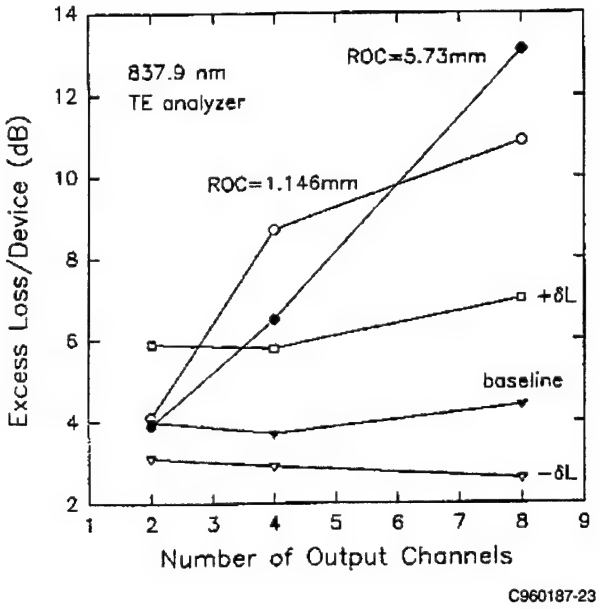

Figure 4-3b. Sample 55B—Splitter Results

The next step was to determine the optimum MMI splitter design. A 1×4×8 splitter was compared to a 1×8 splitter. The designation "1×4×8" refers to a double-staged splitter, which initially splits a single channel into four and subsequently splits each of those four into two, for a total of eight. A 1×8 MMI splitter is a single-stage splitter that goes directly from one channel to eight. The results, accumulated over six different samples, are that the excess insertion loss (over and above the intrinsic splitting loss) ranged from 0.6 to 2.3 dB/channel for the 1×4×8 MMI

splitter, and from 3.2 to 5.2 dB/channel for the 1×8 MMI splitter. Therefore, we conclude that the 1×4×8 MMI splitter is more reproducibly low loss.

We also studied the 2×1 MMI combiners, which are required to recombine the two arms of each Mach-Zehnder interferometer into one channel, and compared them to conventional, low-angle apex recombiners. The mask set included several arrays of four modulators, with two of the four utilizing 2×1 MMI combiners and the other two utilizing conventional, low-angle combiners. The diagram in Figure 4-4 contains a plot of the optical throughput power, extinction ratio, and drive voltage when voltage is applied to each arm of a four-element Mach-Zehnder modulator array, one arm at a time. Only six channels are shown, as the fourth modulator was not functional. The first four channels used MMI combiners, whereas the fifth and sixth used conventional combiners. A clear difference in output power and extinction ratio is observed between channels 1–4 and 5–6. Figure 4-5 shows plots of L-V curves for two modulators, one with an MMI combiner and one with a conventional combiner. The designations NL, NA, TE, and TM correspond to the case where no light is input into the modulator, no polarization analyzer is used in the output, an analyzer is used to look at the TE mode, and an analyzer is used to look at the TM mode, respectively. In the modulator with the MMI combiner, the gradual variation in TM mode with voltage indicates some polarization rotation, probably due to metal-induced stress. The low contrast ratio of the TE mode in the modulator with the conventional combiner indicates depolarization, perhaps induced by the imperfect apex of the combiner. In general, the conventional combiners resulted in a loss about 2–4 dB greater than the MMI combiners.

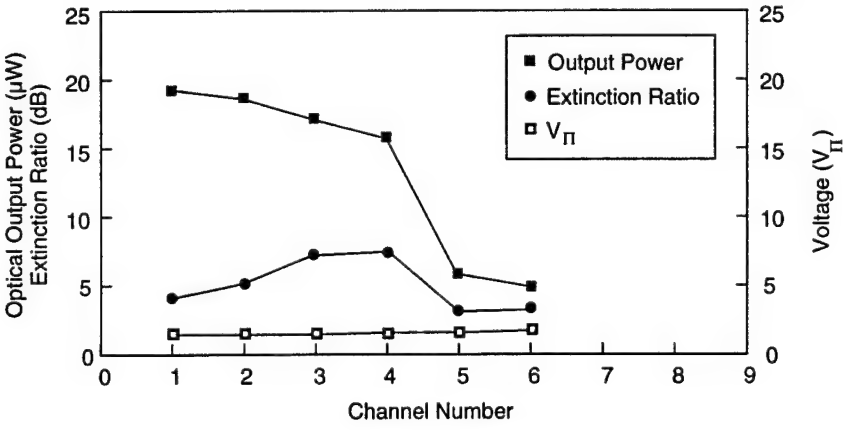

	Channels 1 – 4	Channels 5 – 9
Output Power	20.2 ± 1.7 μW	6.2 ± 0.7 μW
V_Π	1.85 ± 0.01 V	2.01 ± 0.13 V
Extinction Ratio	6.88 ± 1.82 dB	3.8 ± 0.1 dB
Bias Voltage	2.75 ± 0.29 V	2.75 ± 0.35 V

C960187-11

Figure 4-4. Optical Output Power, Extinction Ratio and Voltage Required to Achieve the Full Modulation Depth as a Function of Electrode Number in a Four-Modulator Array

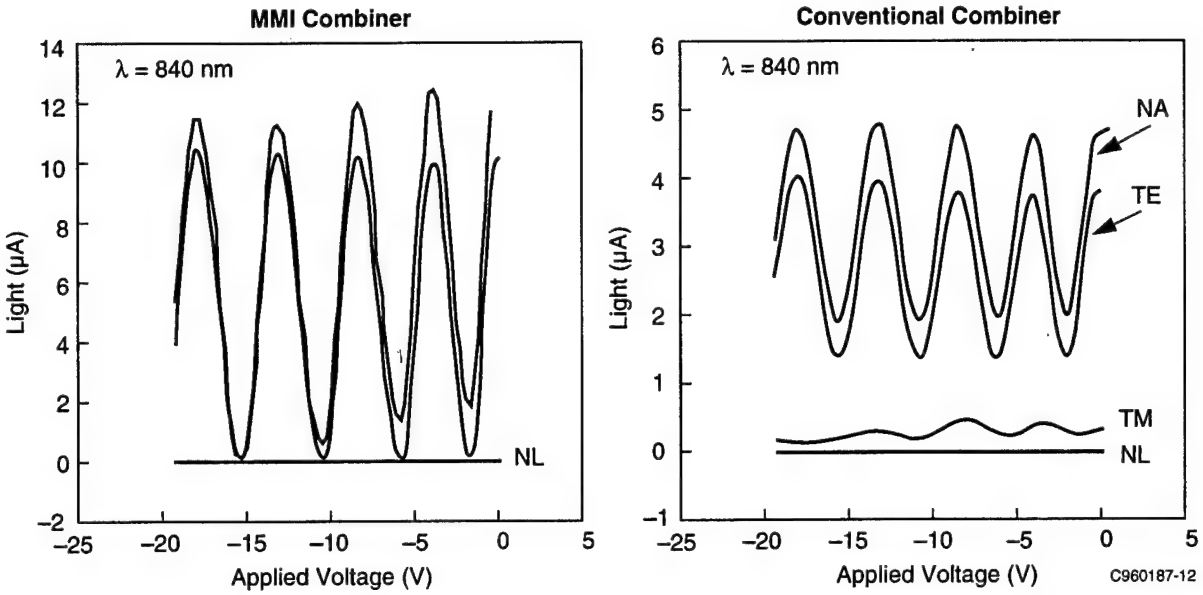

Maximum Output Power: 20 μW
Extinction Ratio: 8.5 dB (23.6 dB)

Maximum Output Power: 6 μW
Extinction Ratio: 3.8 dB (4.0 dB)

Excess Loss: 3–5 dB over MMI

a) Modulator with an MMI Combiner **b) Modulator with a Conventional Combiner**

Figure 4-5. Light Transmitted vs. Applied Voltage

4.1.4 High-Frequency Characteristics of Waveguide Modulators

The high-frequency or microwave characteristics of the modulator were determined experimentally in the 50 MHz to 20 GHz range. As the modulator layout did not incorporate RF probe pads, it could not be tested directly using the standard Cascade Microtech probes. It was thus necessary to provide a temporary package for the modulator to enable the measurements to be performed. Figure 4-6 shows such a package layout wherein standard coplanar RF probe pads on a GaAs substrate were placed in proximity to the modulator chip. The GaAs and modulator chips were both soldered onto the gold-plated brass base plate and the pads connected by means of 0.0007-in-dia gold wires. Several gold wires were bonded together to reduce pad-to-pad lead inductance, whereas vias to ground ensured a low coplanar ground impedance for the RF probe pads on GaAs. As the coplanar RF probe pads on GaAs were measured to exhibit an insertion loss of –0.1 dB and a return loss of –25 dB over a 50 MHz to 40 GHz range, we concluded that this type of packaging provides accurate RF measurements of the modulator characteristics without first needing to de-embed the coplanar RF probes.

The first step in determining the microwave characteristics of the modulator was to measure its small signal input impedance. This was accomplished using a standard Cascade Microtech probe and an HP 8510B network analyzer in the 50 MHz to 20 GHz range, with the modulator biased at each of several different bias voltages. Figures 4-7a and 4-7b show the measured input impedance of the modulator of 3-μm length at bias levels of –7.6 V and –2.8 V, respectively. It is clear from these measurements that at lower microwave frequencies, the modulator behaved like

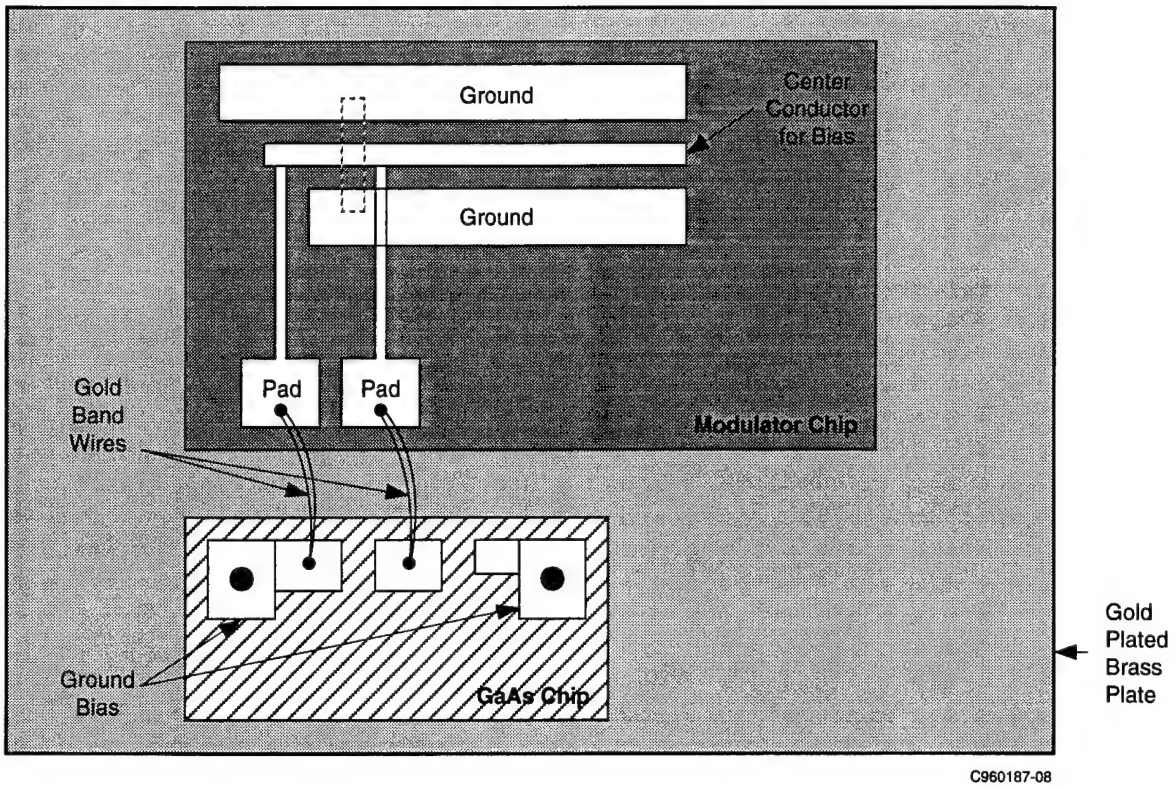

Figure 4-6. Modulator Packaged for On-wafer RF Measurements

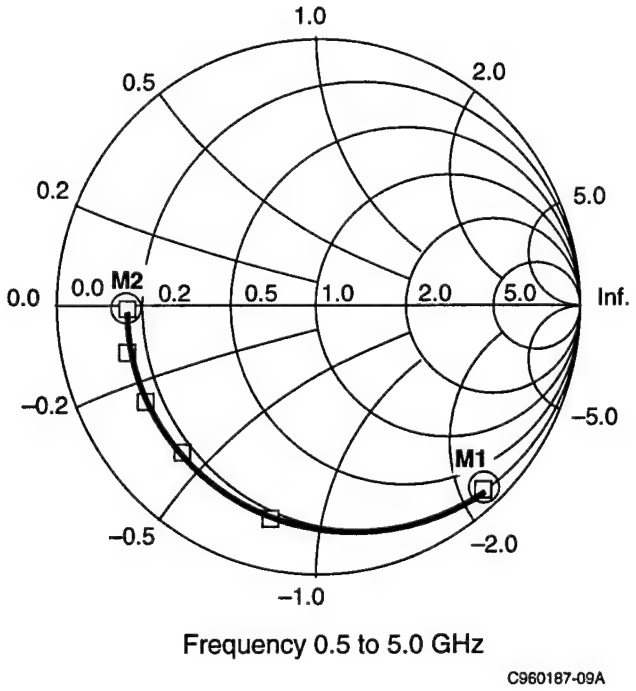

Figure 4-7a. Measured Input Impedance of the Modulator at a Bias of –2.8 V

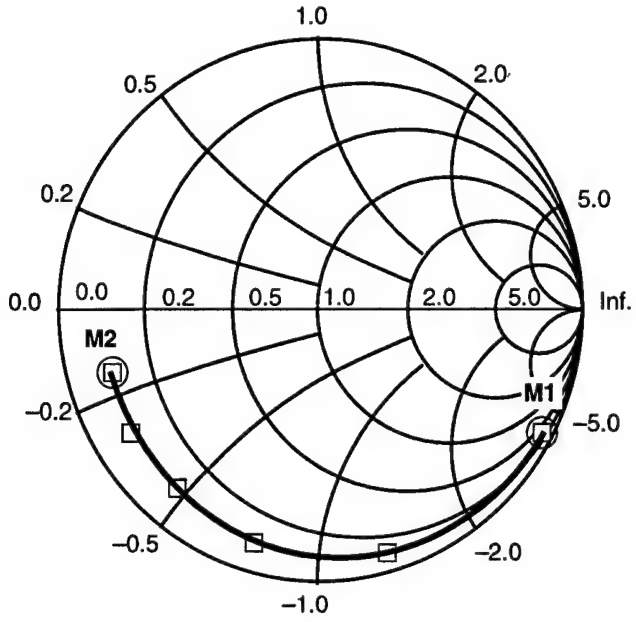

Figure 4-7b. Measured Input Impedance of the Modulator at a Bias of –7.6 V

a lossy capacitor (Figure 4-8a), whereas at high frequencies, it behaved more like a transmission line. Thus, for all practical purposes, the modulator can be modeled as a transmission line (Figure 4-8b).

The next step in characterizing the modulator was to evaluate its microwave performance under normal operating conditions. This was accomplished by using an HP 8702 Lightwave Component Analyzer together with the HP test set in the experimental setup shown in Figure 4-9. The system was first calibrated by using an external light source and the standard HP lightwave receiver. Next, the GaAs modulator was inserted into the optical path as shown, with the microwave signal being injected into the modulator using Cascade Microtech probes. The response of the optical receiver then indicated the RF response of the GaAs modulator. Figure 4-10 shows this response at bias levels of –2.8 V and –7.6 V, respectively. Studying the results shown in Figure 4-10, one notices that the response is practically unchanged for the two bias levels. Furthermore, the output response is not constant, but rather shows a gradual decline of over 15 dB from 0.3 MHz to 3 GHz. A casual observation would indicate that this is indeed the RF frequency response of the GaAs modulator, but a careful study of the results indicates that this is not the case, and that the response is determined to a large extent by the impedance of the RF source. To understand this, one must refer to Figure 4-11, which indicates the modulator being driven by a source of impedance Rs. As the RF modulation efficiency of the modulator is dependent on the RF field strength (Erf), the RF voltage developed across the modulator is an accurate indicator of its efficiency. On the basis of Figure 4-11 and the measured RF input impedance of the modulator, one can easily calculate the complex voltage gain (Vg) for different Rs. These voltage gains are plotted in Figure 4-12, and the curve for Rs = 50 Ω is in excellent agreement with the measured response shown in Figure 4-10. This clearly indicates that the

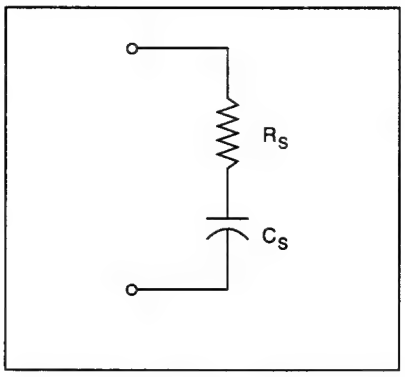

(a) Low Frequency

Figure 4-8a. Low Frequency Equivalent Circuit Model of the Modulator.

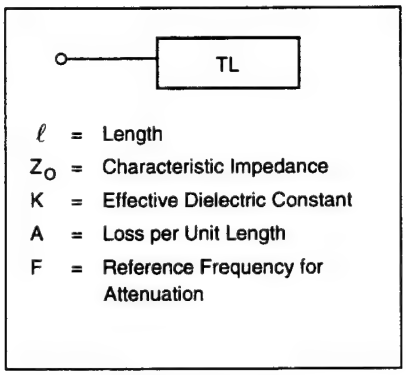

(b) High Frequency

C960187-10

Figure 4-8b. High Frequency Equivalent Circuit Model of the Modulator.

intrinsic RF response of the modulator is constant over the 0.3 MHz to 3 GHz range, whereas the overall RF response is very dependent on Rs and dramatically improves as Rs approaches zero, or a true voltage source. Thus, if higher frequency performance was desired, it would be important to develop an RF driver having as low an impedance as possible.

4.1.5 Modulator Performance vs. Temperature

Because modulators are being developed with the intent of providing an emitter over the full military specification temperature range of –55° to +125°C, tests were carried out to evaluate the performance of the device as a function of temperature. A plot of the optical power transmitted through a Mach-Zehnder interferometric modulator as a function of a single-ended voltage applied to one of the arms is shown in Figure 4-13. Four curves are shown, corresponding to 23°, 50°, 78°, and 100°C. Although the device is clearly operational up to 100°C, the contrast ratio is somewhat degraded over the temperature range. Contrast ratio as a function of temperature (not including the effects of the change in phase) is plotted in Figure 4-14. The ratio degrades from 11.5 dB at room temperature to 6.5 dB at 100°C. Although the goal is for the contrast ratio to be in excess of 10 dB, this modulator would still meet the requirements for link performance over the temperature range tested. Additional measurements have indicated that the change in contrast

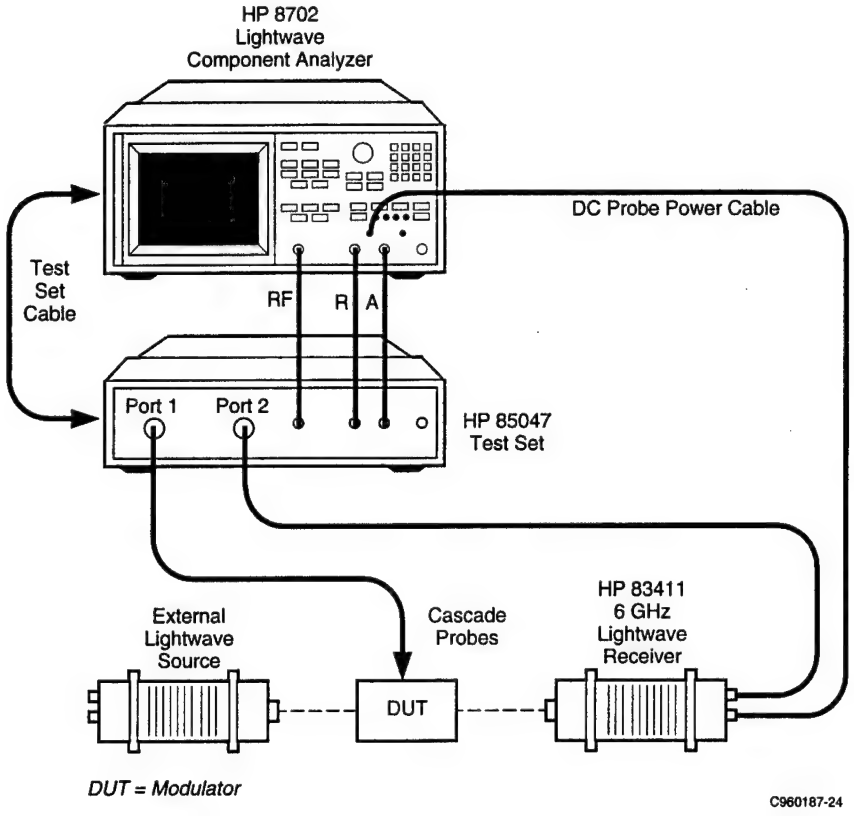

Figure 4-9. Experimental Setup for Measuring the Microwave/Optical Response of the Modulator

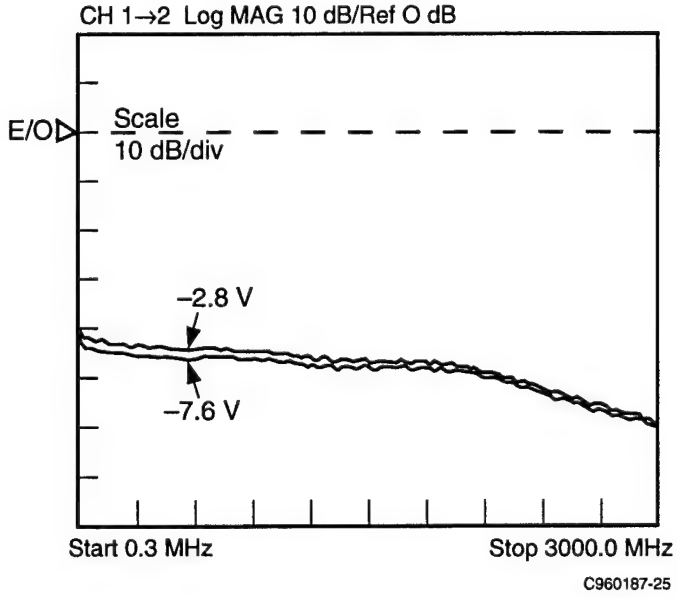

Figure 4-10. Measured E/O Response of the Modulator at a Bias of –2.8 V and –7.6 V

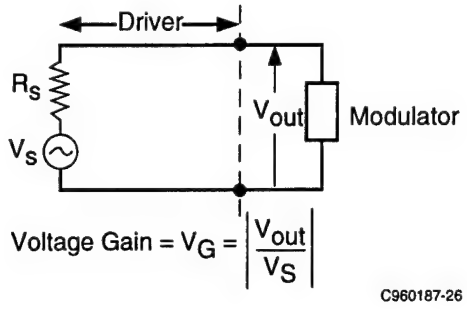

Figure 4-11. Circuit Schematic of a Typical RF Source Driving a Modulator

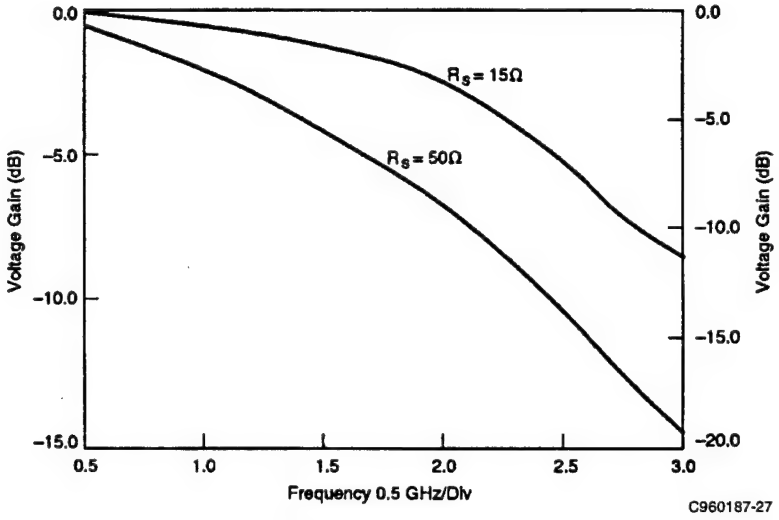

Figure 4-12. Calculated Complex Gain of the Circuit for Various Source Impedances

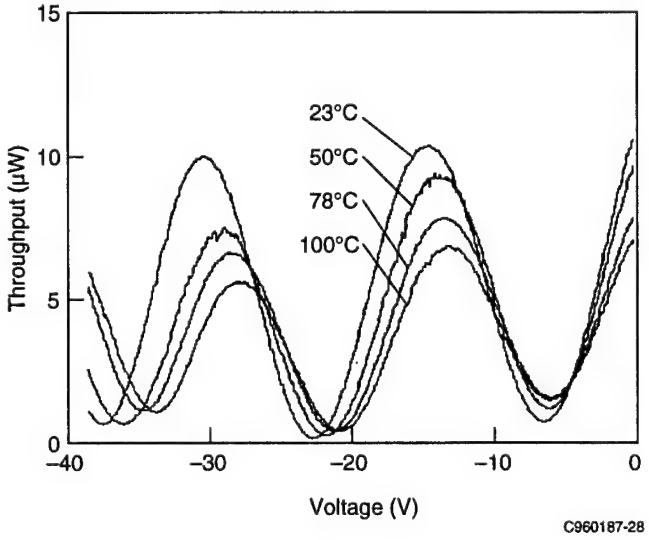

Figure 4-13. Light vs. Voltage for Sample 213 over a 23°–100°C Temperature Range

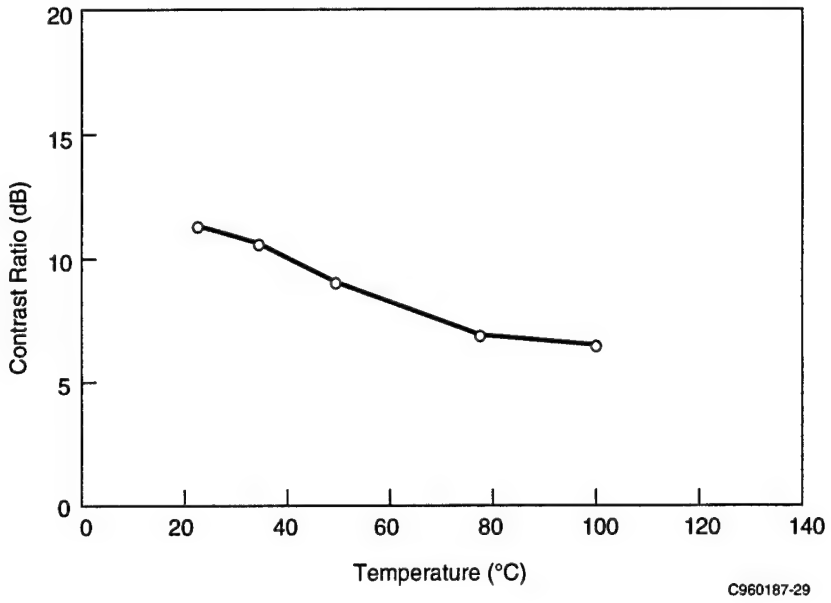

Figure 4-14. Contrast Ratio vs. Temperature for Sample 213

ratio with increasing temperature is a result of a polarization rotation that takes place within the devices and that changes as a function of temperature. We suspected that this is due to residual stress in the device. As the oxide passivation was the most likely source of this stress, new devices were fabricated with the process modified slightly to eliminate the oxide passivation. The performance results at both room and high temperatures are displayed in Figure 4-15. The sample is from the same wafer as that used in Figure 4-13 but with the modified process. The performance over this temperature range is significantly improved. In the region closest to 0 V, which is where the packaged device will be operated, there is less than 1-dB degradation in optical throughput power and contrast ratio remains greater than 10 dB.

4.2 AlGaAs Modulator Array Packaging

4.2.1 Simulation of Expected Performance

To understand the issues and packaging areas requiring most attention, we completed numerical simulations to determine the coupling efficiency and alignment tolerance of the single-mode polarization-maintaining fiber-to-waveguide interface as well as the waveguide-to-multimode fiber interface.

Numerical simulations of the coupling performance between elliptical-core, polarization-maintaining, single-mode fiber and AlGaAs waveguides were carried out by calculating the overlap integral of the mode field profiles of the fiber and the waveguide. The simulated mode mismatch loss, using the current waveguide design parameters and D-fiber mode field profile, is 0.7 dB. Tolerance misalignments of 1 dB could be extracted from the simulation and were found to be ±0.47 μm in the transverse direction and ±0.55 μm in the lateral direction. The longitudinal tolerance (1 dB) was found to be +3.85 μm, with a periodic ($\lambda/2$) 0.77-dB difference in the min/max due to the Fabry-Perot effect. Measurements of the coupling efficiency and 1-dB

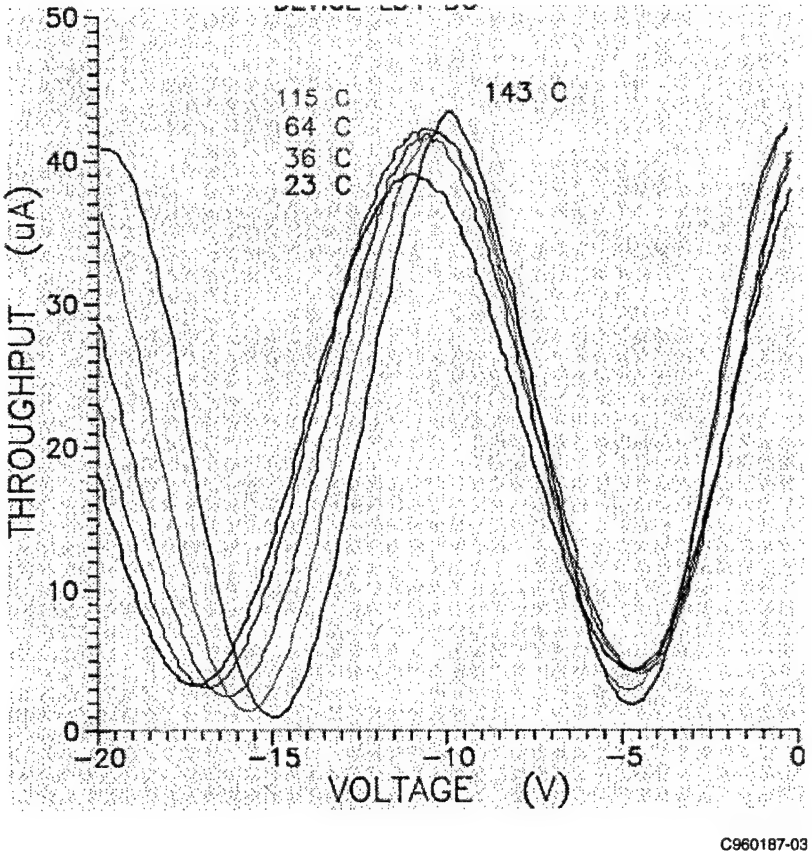

Figure 4-15. Light vs. Applied Voltage for Sample 273A, Device L34 D6

displacement tolerances have been made using an unoptimized AlGaAs waveguide. The lateral, transverse, and longitudinal tolerances were ±0.48 μm, ±0.31 μm, and +2.45 μm, respectively. The coupling loss due to mode mismatch was 1.02 dB. This experimental result was arrived at by numerically factoring out both the Fresnel loss at two AlGaAs/air interfaces and the measured waveguide attenuation.

Calculations were also done to determine the coupling efficiency between the AlGaAs waveguides and the multimode fiber (SpecTran SG508) used in the fiber ribbon cable. Because there is a large numerical aperture mismatch between the waveguide (≅0.4) and the fiber (0.275), optical losses will occur. It was decided to use lensed fibers to reduce this loss.

4.2.2 Optical Subassembly Packaging Results as a Function of Temperature

Several waveguides or modulators were optically packaged by aligning a single-mode polarization-maintaining fiber to the input of the chip using the baseline approach described above. As part of the evaluation, different adhesives were examined. A desirable adhesive will have a low coefficient of thermal expansion (CTE), low shrinkage during cure, and will cure quickly and operate over a wide temperature range without losing strength. Temperature performance measurements of optically packaged subassemblies were conducted to evaluate the stability of the single-mode fiber connection to the modulator. The packaged assembly was placed on a thermal-electric heater/cooler and the change in throughput power was recorded. The

assumption is that the change in throughput power is due to temperature-induced optical misalignments. Figure 4-16 shows the relative change in optical coupling over a 115°C temperature range. The lower temperature limit was due to the limitations in the experimental setup. The upper temperature roll-off is due to expansion of the epoxy. Our results to date were made using low-shrinkage, moderate CTE epoxies. Other epoxies with lower CTEs have been considered but take many hours to cure.

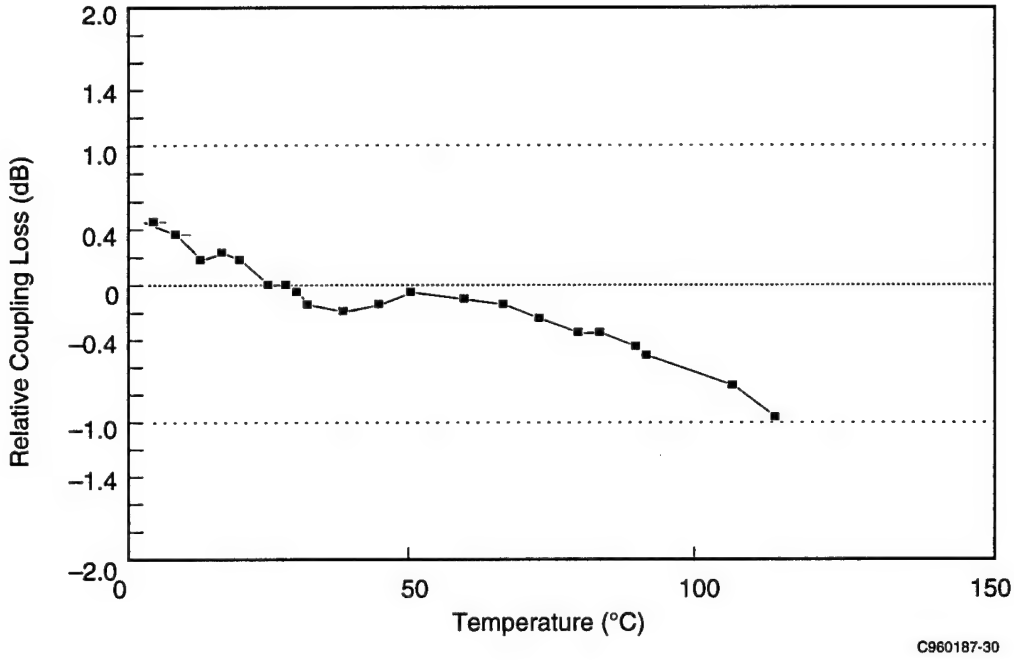

Figure 4-16. Change in Input Coupling Loss vs. Temperature

4.2.3 DC Characterization of a Waveguide-Modulator-Based Package

A photograph of the completed modulator package is illustrated in Figure 4-17. A lead frame package is used, with the wall of the package cut away at two points to allow the single-mode input fiber and multimode output fibers to enter and leave the package. The optical subassembly, including the modulator array chip, the alumina submount for the single-mode fiber, and the silicon V-groove assembly containing the multimode fiber, is visible at the top of the package. DC testing was carried out with this package, with the stability of the coupling efficiencies at the fiber-modulator interfaces evaluated over temperature. It was originally planned that high-speed test boards would be provided by Martin Marietta, but due to cost growth problems at Martin Marietta, that task was eliminated. Therefore, high-speed testing could not be performed on the packaged modulator-based transmitters.

Table 4-1 contains a summary of the loss budget of packaged modulators. The power input to the polarization-maintaining fiber from the pigtailed laser is 31 mW. The power output from the multimode fibers coupled to the output of the modulator array channels ranged from 36 to 70 μW. This corresponds to a total insertion loss ranging from 29.4 to 26.5 dB, of which 6 dB corresponds to the intrinsic splitting loss associated with distributing a single input channel

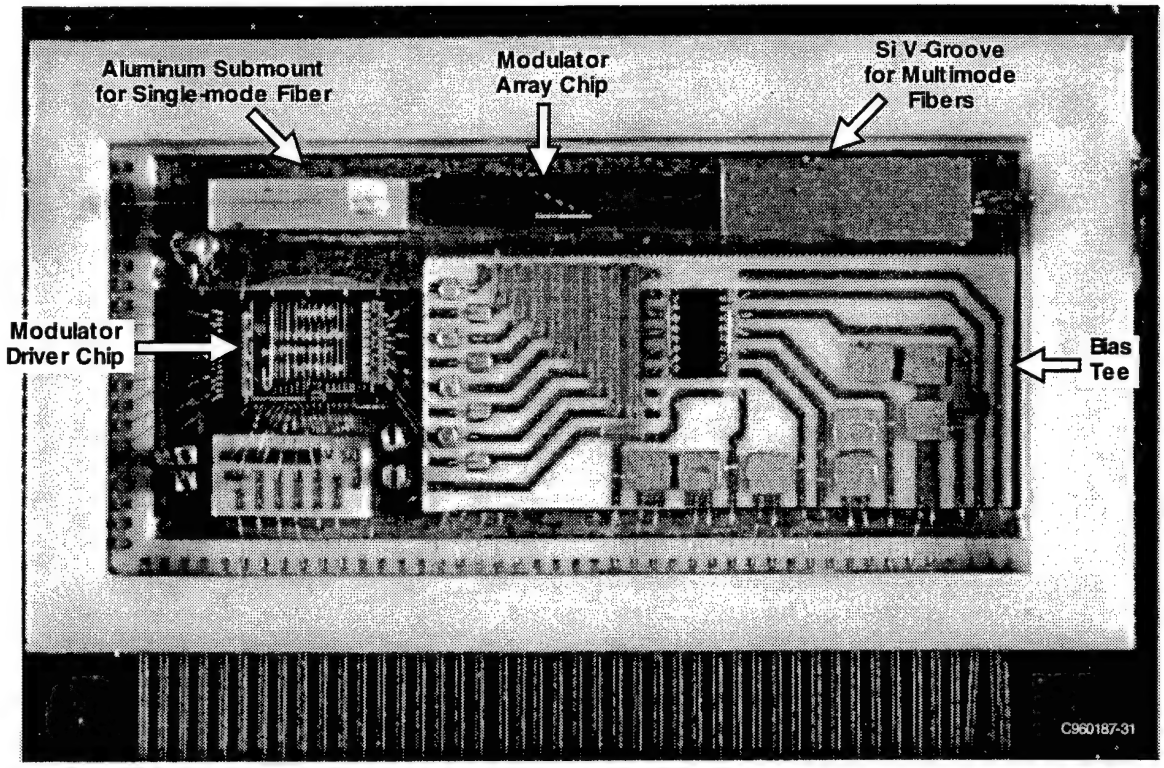

Figure 4-17. Completed Waveguide-Modulator-Based Package

Table 4-1. Loss Budget Packaged Modulator 212C L2-3

Output from pigtailed laser	31 mW	14.9 dBm
Output power from pigtailed modulator		
Channel 1	0.06 mW	–12.2 dBm
Channel 2	0.07 mW	–11.6 dBm
Channel 3	0.062 mW	–12.1 dBm
Channel 4	0.036 mW	–14.4 dBm
Subassembly loss:	min	26.5 dB
	max	29.4 dB

among four output channels. This leads to the conclusion that there is 20 to 23 dB of excess loss. The contributions to this loss include optical absorption in the waveguide, additional absorption loss due to the metal electrode deposited on the waveguide, excess splitting loss due to imperfect splitters, coupling loss between the single-mode fiber and the waveguide array, and coupling loss between the waveguide outputs and the multimode fiber.

Figure 4-18 displays the I-V characteristics of the packaged modulator under reverse bias. The leakage current is on the order of 40 μA at –8 V, which is an acceptable level. The optical throughput of the modulator versus applied voltage is displayed in Figure 4-19. The maximum output is at 0 V, whereas the minimum occurs around 7.5 V. A 3-dB extinction ratio is observed. This is smaller than that observed from the same modulator unpackaged. We attribute the

degradation of the extinction ratio to stress induced by the packaging. We had previously seen degradation in contrast ratio due to stress arising from a dielectric coating. However, the voltage length product, 22.5 V-mm, is well within the range of values we have previously observed and that would be expected.

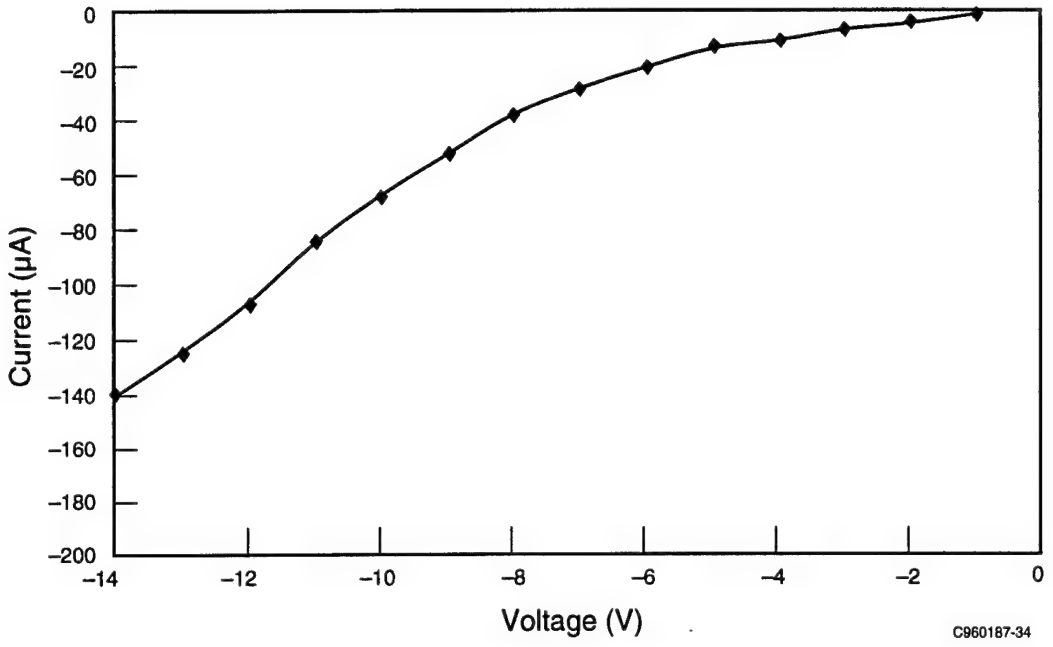

Figure 4-18. Reverse Bias Characteristics of Mach-Zehnder Waveguide Modulator

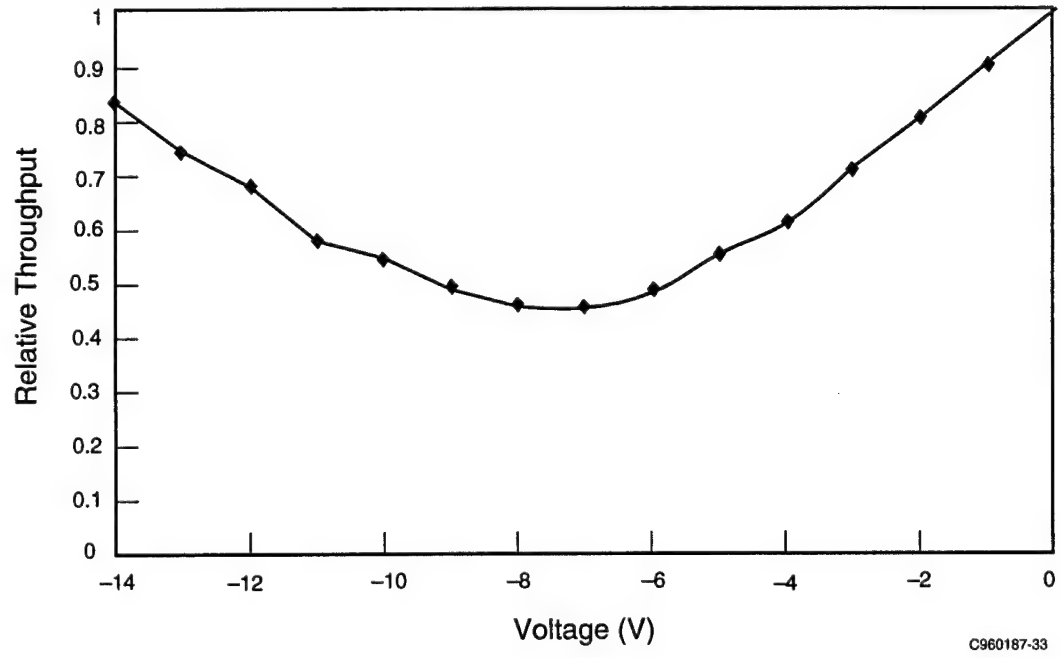

Figure 4-19. Modulator Optical Throughput vs. Applied Voltage

Figure 4-20 illustrates the degree of robustness versus temperature achieved in the packaged system. The relative throughput change was measured over –15° to +70°C and normalized to the throughput at room temperature (20°C). The throughput was found to increase by about 0.5 dB at –15°C, and decrease by about –2.3 dB at 70°C. The degradation in throughput is due to shifts in the relative positions of input and output fibers with respect to the modulator array, plus any degradation in throughput observed on the chip itself, but is probably dominated by the coupling between the single-mode fiber input and the array.

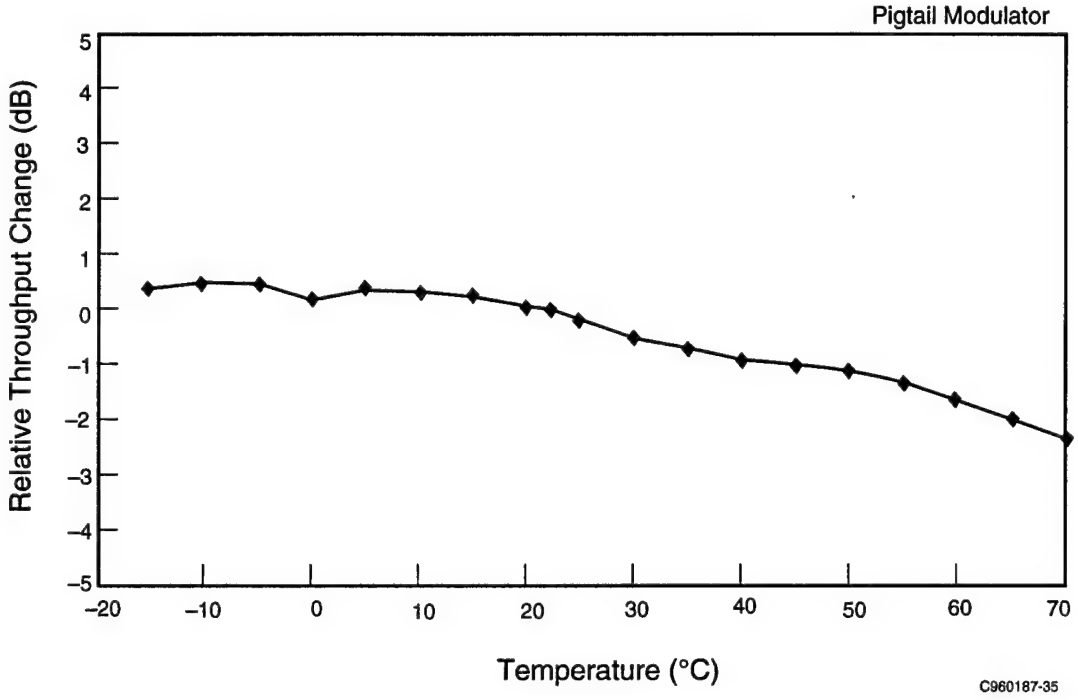

Figure 4-20. Optical Throughput vs. Temperature for a Waveguide Modulator Array Packaged with Single-Mode Fiber Input and Multimode Fiber Output

4.3 Polymer Backplane Development

4.3.1 Optical Waveguide Results

The glass:polyimide board materials chosen as the baseline backplane material have rough surfaces, which are not conducive to the fabrication of low optical loss waveguides. Examination of typical laminated boards reveals a periodic undulation in surface height resulting from the wave of the glass fiber cloth in the laminate. Figure 4-21 illustrates the surface roughness of an "as-received" glass:polyimide substrate from which the rolled copper coating has been chemically etched. Peak-to-peak roughness of 2.2 μm is observed. Note also the relatively high-frequency components of the roughness. The rapid undulations in surface height are expected to cause significant optical loss. We have characterized a number of planarizing polymers for deposition on the board before the deposition of the waveguides. Of the materials evaluated, the most promising is a Dow benzocyclobutene (BCB) material. This material was designed to have good planarization capabilities (91-99% degree of planarization) for electronic packaging

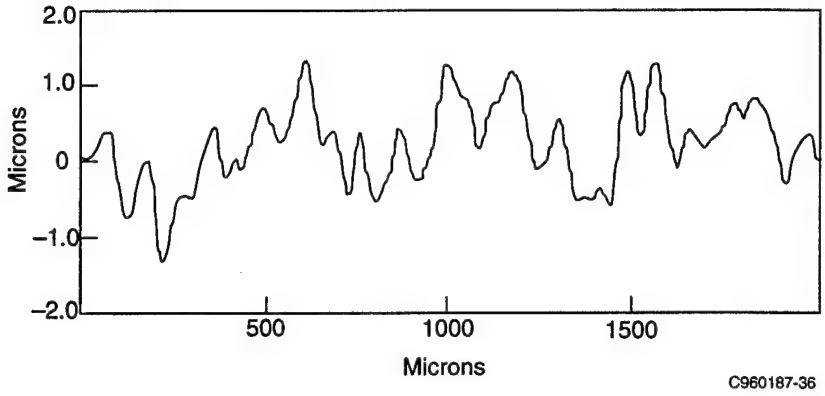

Figure 4-21. Surface Roughness of an "As Received" Glass:Polyimide Substrate

applications. To evaluate the loss resulting from fabrication of polyimide waveguides on glass:polyimide boards planarized with this material, 4.0-μm-thick films of polyimide were deposited on oxidized silicon wafers and also on glass:polyimide substrates that had been planarized with BCB (5-μm thickness). Figure 4-22 illustrates the resulting variation in surface height. Note that the peak-to-peak height variation has been reduced to less than 0.5 μm, and the high-frequency variations have been eliminated. The additional loss associated with fabricating the waveguides on glass:polyimide substrates rather than the optically smooth oxidized silicon was determined to be 0.4 ± 0.6 dB/cm.

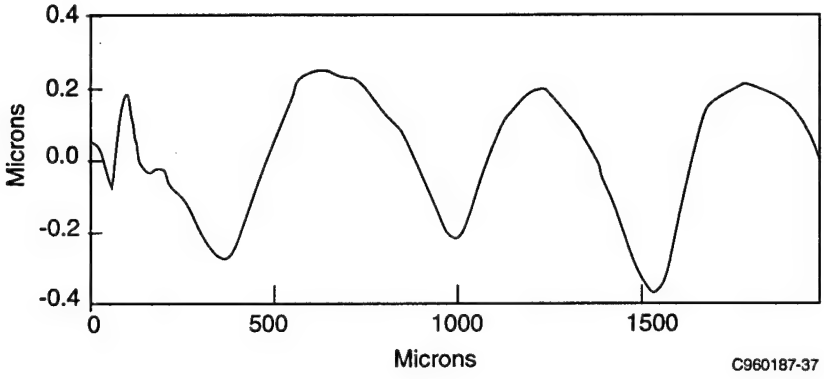

Figure 4-22. Variation in Surface Height of Glass:Polyimide Substrate after Planarization with BCB

We also acquired data relating to the excess loss of waveguide bends as a function of the radius of curvature, information that was then used to design the final demonstration experiment. Bends with radii of curvature ranging from 0.5 to 10 mm were measured. Although there was a fair amount of scatter in the data, the best results were achieved for 4 to 6 mm bend radii, where the excess insertion loss ranged from 0.1 to 0.7 dB.

4.3.2 Optical Channel Cross-Talk Measurements

An experiment was carried out to evaluate the density of channels that can be accommodated by a single expanded beam connect, as illustrated in Figure 3-5 and described above. Polyimide waveguides were fabricated on a silicon substrate, and a pair of half-GRIN lenses were placed into the alignment marks on the silicon substrate such that they coupled light from one array of waveguides into another array of waveguides. The crosstalk was measured as a function of displacement from the axis by measuring the output from channel n′ and n+1′ for input into channel n. Figure 4-23 shows the resulting crosstalk for a single lens pair. For the 3-mm dia lens, an optical crosstalk of better than –20 dB is maintained over a total distance of 1.8 mm. We note that the best crosstalk figure obtained for any lens pair to date has been –37 dB. The waveguide dimensions for this experiment were 15 μm by 15 μm, with a 15μm gap, for a pitch of 30 μm. This would imply that a single lens pair could be used to couple up to 60 waveguide channels from one board to another with better than 20 dB crosstalk with the stated dimensions, or that 45 guides of our target dimensions of 25 μm by 25 μm with a 15μm gap could be used. Note that in a typical implementation, the optical signal would pass from the source board to the backplane, and then to a second board; thus the optical crosstalk figure for a complete interconnect with two connectors would be –17 dB, translating to an electrical crosstalk of –34 dB, or 20-mV crosstalk noise per 1 V of signal.

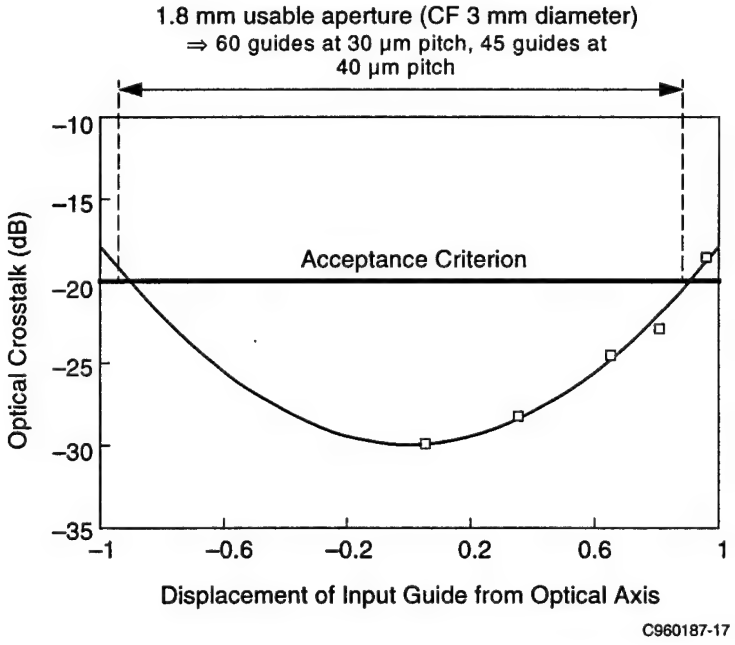

Figure 4-23. Crosstalk vs. Waveguide Position for a Board-to-Backplane Connector

4.3.3 Fabrication of Connector Fixtures

Our baseline design for the board-to-backplane connector employs a half-GRIN lens pair connecting arrays of waveguides using expanded-beam techniques. Fixtures locate the GRIN lenses to both the boards and backplanes. The fixture, illustrated in Figure 4-24, provides for the 90° turn of the light beam required to move the signal from board to backplane. The lenses are

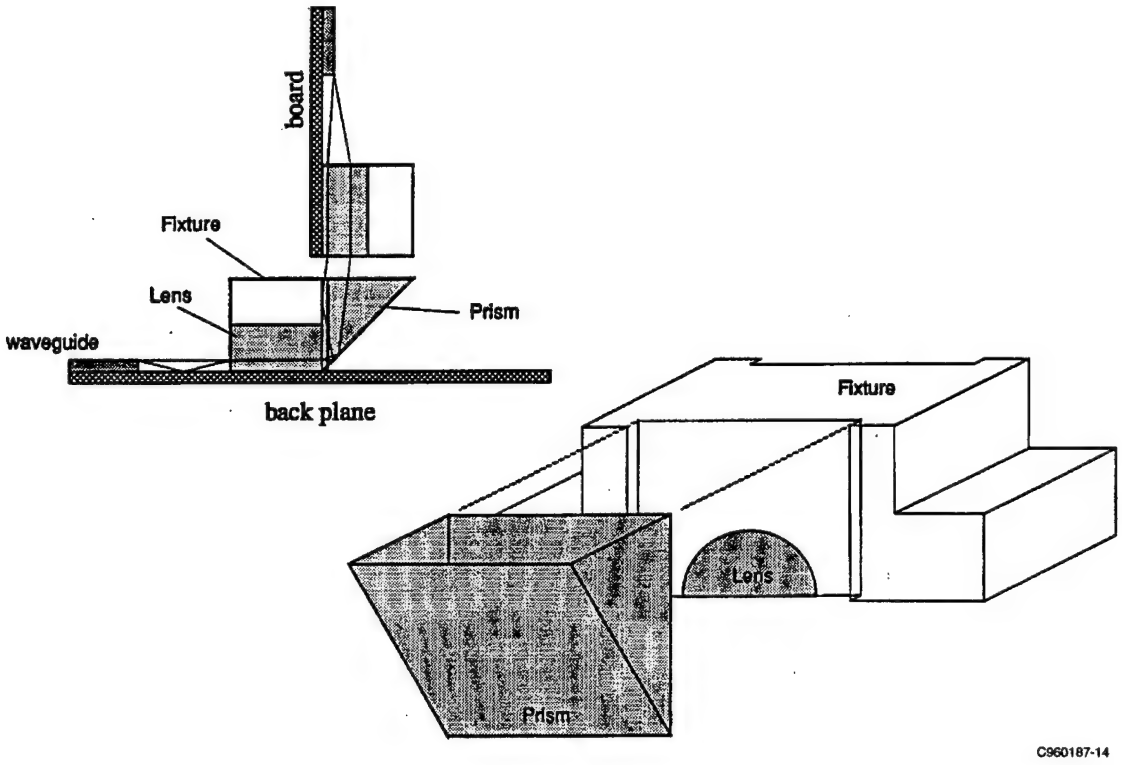

Figure 4-24. A Diagram of the Fixture being Fabricated to Provide Alignment Between Polymer Waveguides, GRIN Lens for Expanded-Beam Connectors, and 45° Coupling Prism

passively aligned with respect to the endface of the waveguide by structures defined on each board. The fixture fits over the half-GRIN lenses and aligns a 45° prism to the lens. The prism provides the 90° turn of the light beam. The lenses are derived from commercially available optics. The fixtures have been produced from a machinable ceramic. For full-scale production, the ceramic fixtures would be molded and processed using established techniques similar to those employed in the manufacture of ferrules for fiber-optic connectors.

4.3.4 Board-to-Backplane Demonstration and Assessment of Alignment Tolerances

The backplane demonstration consisted of two boards containing polymer waveguides and the GRIN-lens-based expanded-beam connectors and associated fixtures described above. The purpose of the demonstration was to understand the tolerance of such a connector to misalignment and to show the transfer of signal from the optical input of one board to the optical output of the other. The experimental setup was described previously and illustrated in Figure 3-7. The results are illustrated in Figure 4-25. The boards were mounted on micropositioners, and the decrease in throughput as a function of misalignment was measured. If the criterion is that misalignment contributes less than 1 dB additional loss, then it was observed that the translational alignment should be maintained to within +0.37/–0.25 mm. As the tolerance should be symmetrical, the discrepancy is probably due to experimental error. When the same criterion is applied to rotational alignment, it is found that a misalignment of +0.19/–0.15 degrees can be

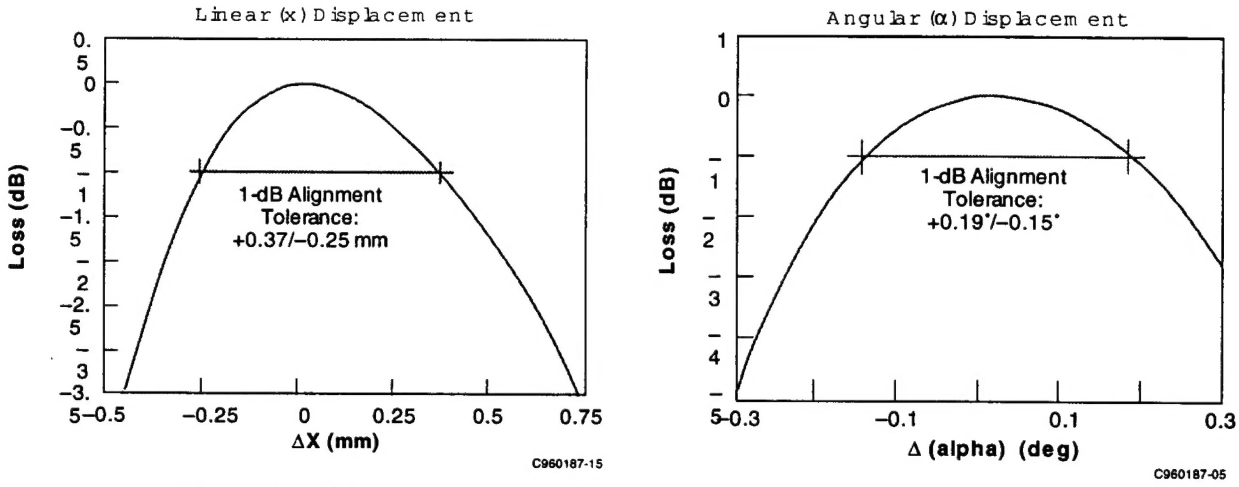

a. Linear (x) displacement **b. Angular (α) displacement**

Figure 4-25. Results of Polymer Backplane Experiment

tolerated. This reduced tolerance to rotational misalignment is by design. Translational tolerance is achieved at the expense of rotational tolerance, but that the latter is expected to be easier to control in a backplane configuration.

Other measured results from this demonstration include a waveguide propagation loss of 0.3 dB/cm and a connector loss of 3.4 dB. As described in Section 4.3.2, up to 36 channels can be coupled from one board to the other within the space of a connector based on a 3-mm dia GRIN lens with ≤20 dB optical crosstalk.

4.4 Vertical-Cavity Surface-Emitting Laser Development

When this task was initiated, Honeywell had demonstrated VCSELs under another program where the goal was to integrate VCSELs with photodetectors and field-effect transistors (FETs). The structure was therefore slightly different than what is optimum for OETC. Integration necessitated the use of a semi-insulating substrate, so to make contact to the n-side of the junction, a special thick n-doped contact layer was included in the cavity such that the cavity becomes three wavelengths thick. To make contact to this layer, we etch down to it, thus creating a mesa structure. Because integration with dissimilar devices is not required as part of OETC, we can migrate our structure toward one that is planar. The device can be grown on a conducting substrate, and a common contact can be made by depositing metal on the back side of the wafer. The mesa etch is not required.

We have therefore chosen to use a process similar to AT&T's VCSEL process. This involves using proton implantation to provide current confinement, a broad-area ohmic contact on the back side of the wafer, and a circular ohmic contact on the top side. The two structures were illustrated in Figure 3-7. Under this program (OETC-1), we implemented some of the steps required to migrate to this structure. We removed the contact layer from the cavity so that the total cavity thickness was equal to one wavelength and put a broad area contact on the back side of the wafer. We temporarily continued to use the mesa etch to provide current confinement. We

also increased the composition of the cladding layers in the cavity to improve the performance as a function of temperature. VCSELs were successfully fabricated with this structure that showed improved performance over temperature. Light and voltage versus current curves are shown in Figure 4-26. The additional steps required to migrate to the structure to be used for OETC arrays will be carried out under OETC-2.

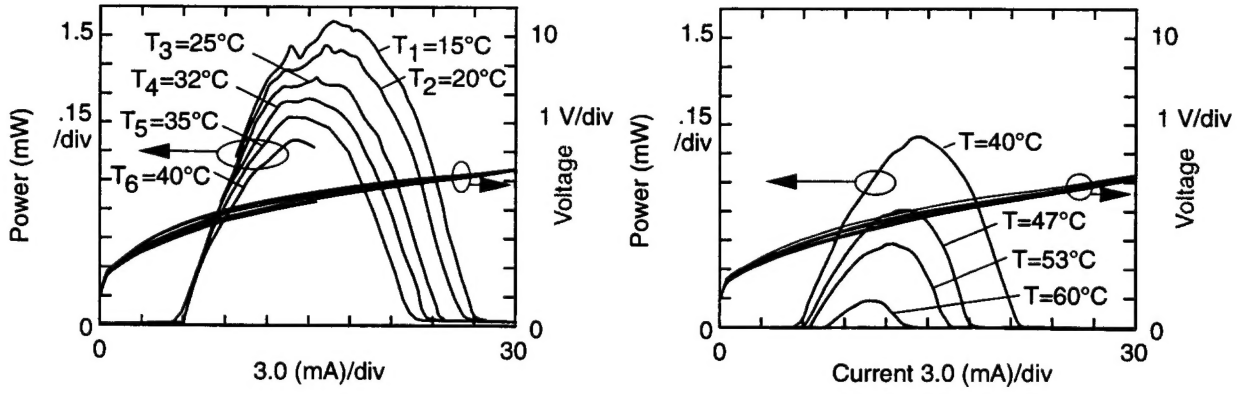

Figure 4-26. Temperature Performance of Integrable VCSELs

We also investigated the origin of the high resistance of our devices and believe it to lie in the top p-ohmic contact. Experiments were carried out to increase the doping of the top contact layer. We discovered that increased Zn doping seemed to have a negative effect on contact resistance. Subsequent investigation revealed that Zn doping in layers containing high Al led to those layers becoming relatively resistive and resulted in higher resistance ohmic contacts. We will continue to investigate the optimum doping profile in the contact region.

Section 5
Summary

The major results of this work are as follows.

Waveguide Mach-Zehnder interferometric modulators have been fabricated in AlGaAs materials. Compact structures can be fabricated using a deep waveguide etch and multimode interference splitters and combiners. We determined that a p-i-n structure provided voltage-length product in the range of 20-25 V-mm compared to 50 V-mm for an undoped structure. This higher drive efficiency was achieved with a mild penalty in passive waveguide optical loss (about 1 dB/cm). Extinction ratios in excess of 10 dB can be readily achieved. We also demonstrated that devices can be operated to greater than 143°C with very little change in maximum output power or extinction ratio; however, the device performance is very sensitive to details of device fabrication. For instance, the insertion loss of the multimode interference splitters and combiners is sensitive to just a few tenths of a micron variation in waveguide width. Insertion loss and extinction ratio of the active modulator are very sensitive to stress induced by dielectric or metal layers. The size of the device will make large arrays (>4) difficult to produce with reasonable yield. On the other hand, due to the reverse-biased operation, when properly fabricated, waveguide modulators are likely to operate and be more reliable at higher temperatures than lasers would be.

We have also demonstrated packaging techniques for providing both single-mode polarization maintaining fiber input and multimode fiber outputs for a waveguide modulator array. With proper attention to submount materials, dimensions, and adhesives, coupling efficiency variations of less than 1 dB can be achieved between 0° and 110°C; however, the packaging is very labor intensive, requiring active alignment of the fibers at both input and output and grinding of substrates to a specified thickness. The vendor performing pigtailing of the CW laser that provides the input optical beam had a great deal of difficulty delivering a properly pigtailed laser. Here, again, we discovered that stress induced by the packaging could have a dramatic effect on modulator performance.

The polymer waveguide backplane experiment demonstrated that a single expanded-beam connector can provide a high density of board-to-board connections. Required alignment tolerances were found to be consistent with typical fabrication tolerance for boards and chassis. Low-loss waveguides can be fabricated on standard board materials with reasonable optical loss. The required fabrication processes and alignment tolerances seem to be consistent with what will be required for cost-effective fabrication of board-level waveguide-based optical interconnects.

The work reported here, as well as a substantial amount of other work in VCSEL fabrication carried out at Honeywell, leads us to believe that VCSELs will be a much more cost-effective approach to parallel optical links than will waveguide modulators. Promising data in the high-temperature performance of these devices has also been collected, although waveguide modulators probably still have the edge in this regard. It seems very probable that performance and reliability will be adequate for commercial application of VCSELs to parallel links, but further work will be required to determine if the devices possess sufficient reliability to operate over the full military specification temperature range.

Honeywell

LETTER OF TRANSMITTAL

29 April 1996 Tally F3592

Ship To: Advanced Research
Projects Agency (ARPA)
3701 North Fairfax Drive
Arlington, VA 22203-1714

Attention: ARPA/OASB/Library

Contract Number: MDA972-92-C-0071
OETC

In accordance with the Terms and Conditions of the DD Form 1423 we are hereby submitting:

Quantity Shipped:	Description:
1 Lot	CLIN 0001: Research
(1 Copy)	A004: Final Technical Report for the period 01 July 1992 through 30 April 1995.

Should you have any questions concerning this submission, please contact us at:

Honeywell Inc.
Honeywell Technology Center
Contract Management MN65-3415
3360 Technology Drive
Minneapolis, MN 55418

Phone: 612/951-7190
Contract Data Management

Distribution:

Dr. A.Yang, ARPA/MTO	2 Copies
ARPA/OASB/Library	1 Copy
Defense Tech. Info. Ctr.	2 Copies
Darlene West, MN65-3415	Ltr Copy